Numerical Study of High Spectral Efficiency and High Temperature Energy Harvesting Metamaterial Emitter to Improve Thermophotovoltaic performance

Sifan Tamiru Tefera

A Thesis Submitted to the Department of Applied Physics

School of Applied Natural Science

Presented in Partial Fulfillment of the Requirements for the Degree of Master's in Applied Physics (Material Physics)

Office of Graduate Studies

Adama Science and Technology University

June, 2022

Adama, Ethiopia

Numerical Study of High Spectral Efficiency and High Temperature Energy Harvesting Metamaterial Emitter to Improve Thermophotovoltaic performance

Sifan Tamiru Tefera

Advisor: Fekadu Tolessa (PhD)

Co-advisor: Demise Jobir (PhD)

A Thesis Submitted to The department of Applied Physics

School of Applied Natural Science

Presented in Partial Fulfillment of the Requirements for the Degree of Master's in Applied physics (Material Physics)

Office of Graduate Studies

Adama Science and Technology University

June, 2022

Adama, Ethiopia

Declaration

I declare that this Master thesis entitled **"Numerical Study of High Spectral Efficiency and High Temperature Energy Harvesting Metamaterial Emitter to Improve Thermophotovoltaic performance"** is my own work and has not been submitted to any university for similar purpose. The references used in this proposal are duly recognized by proper citations.

__________________________ _________________________ _________________

Name of student Signature Date

Recommendation

I/we, the advisor(s) of this thesis, hereby certify that I/we have read the revised version of the thesis entitled **" Numerical Study of High Spectral Efficiency and High Temperature Energy Harvesting Metamaterial Emitter to Improve Thermophotovoltaic performance"** prepared under my/our guidance by **Sifan Tamiru Tefera** submitted in partial fulfillment of the requirements for the degree of Mater's of Science in Applied Physics Therefore, I/we recommend the submission of revised version of the thesis to the department following the applicable procedures.

________________	________________	________________
Major Advisor	Signature	Date
________________	________________	________________
Co-advisor	Signature	Date

Approval Page

We, the advisors of the thesis entitled **"Numerical Study of High Spectral Efficiency and High Temperature Energy Harvesting Metamaterial Emitter to Improve Thermophotovoltaic performance"** and developed by **Sifan Tamiru Tefera,** hereby certify that the recommendation and suggestions made by the board of examiners are appropriately incorporated into the final version of the thesis.

___________________	___________________	___________________
Major Advisor	Signature	Date
___________________	___________________	___________________
Co-advisor	Signature	Date

We, the undersigned, members of the Board of Examiners of the final open defense by Sifan Tamiru have read and evaluated his thesis entitled "Numerical Study of High Spectral Efficiency and High Temperature Energy Harvesting Metamaterial Emitter to Improve Thermophotovoltaic performance" and examined the candidate. This is, therefore, to certify that the thesis has been accepted in partial fulfillment of the requirement of the Degree of Master's.

___________________	___________________	___________________
Chairperson	Signature	Date
___________________	___________________	___________________
Internal Examiner	Signature	Date
___________________	___________________	___________________
External Examiner	Signature	Date

Finally, approval and acceptance of the thesis is contingent upon submission of its final copy to the Office of Postgraduate Studies (OPGS) through the Department Graduate Council (DGC) and School Graduate Committee (SGC)

___________________	___________________	___________________
Head of Department	Signature	Date
___________________	___________________	___________________
School Dean (SoANS)	Signature	Date
___________________	___________________	___________________
Office of Postgraduate Studies, Dean	Signature	Date

Acknowledgment

First and for most, I am grateful for his love and kindness of the Almighty God in giving me health, strength, patience and protection throughout my study of this work. Next, I am grateful thanks to my advisor Dr. Fekadu Tolessa for sharing useful skill, experience, and for his good interpersonal relationship as well as sharing of his precious time to read and comment this thesis paper. Also I would also like to thank to my Co-advisor Dr. Demise Jobir. Finally, I would like to give a deepest gratitude to Adama Science and Technology University, School of Applied Natural Science, Department of Applied Physics program for providing me with a grant that helped me to carry out this thesis work.

Contents

List of figure

List of Table

List of acronyms

BB……………………………Black body

E_g……………………………..Energy band gap

EQE…………………………...External quantum efficiency

IQE…………………………...Internal quantum efficiency

MM……………………………Metamaterial

MP…………………………….Magnetic polariton

TPV…………………………...Thermophotovoltaic

PV……………………………..Photovoltaic

SPP……………………………Surface plasmon polariton

SPV…………………………....Solar thermophotovoltaic

λ_c……………………………….Cut-off wavelength

Abstract

In this work, a broad band and wide angle selective nano-pyramid metamaterial emitter was designed and analyzed. The selective nano-pyramid metamaterial emitter was designed from tungsten and aluminum nitride using COMSOL Multiphysics software. To obtain broadband emission of the emitter, the geometric parameters such as the base length of the pyramid, height of the pyramid, and thickness of dielectric were optimized while the parameters such as width of the unit cell and ground thickness of tungsten were fixed. The numerical simulation showed high emissivity below the cutoff wavelength when the geometric parameters were fixed at w = 395 nm, h_3 *= 260 nm,* h_1 *= 160 nm,* h_2 *= 80 nm, and* b_1 *= 215 nm. In this study, a high average of emissivity of about 0.964 was achieved below the cutoff wavelength (0.1 µm-2.2 µm), whereas the emissivity was dramatically reduced above the cutoff wavelength. The emissivity below cutoff wavelength was obtained because of the excitation of magnetic polariton and surface plasmon polariton. Furthermore, the designed metamaterial emitter was polarization independent and achieved high emissivity over a wide range of incident angles from* 0^0 *to* 60^0*. Moreover, the designed emitter has a higher spectral efficiency than the blackbody for EQE of InGaAs and maximizes the efficiency of the TPV system by 9.3, 5.3, 3.68, and 3 times the blackbody spectral efficiency at 900 K, 1000 K, 1100 K, and 1200 K. Additionally, this emitter had a higher spectral efficiency than Jiang et al. (2019) and black body for EQE of InGaAsSb. Generally, the designed selective nano-pyramid emitter was obtained with 75% and 86.2% spectral efficiency for InGaAs band gap energy (0.55 eV) at 1200 K and 1600 K, which was higher than blackbody and previous scholars.*

Keyword*: Thermophotovoltaic system; Metamaterial; Emitter; cut-off wavelength; emissivity*

1. Introduction

1.1. Background

Energy is life since we all require it, and it is a source of advancement. As a result, in order to contribute to the planet's long-term sustainability in the face of the climate issue, we are moving forward, together, toward a new energy. Renewable and non-renewable energy are the two basic types of energy. Non-renewable energy resources are in short supply, due to the fact that they require a long time to refill. These non-renewable resources have the advantage of allowing power plants to produce more power on demand. On the other hand, renewable resources are self-renewing. Sunlight, wind, rain, tides, waves, and geothermal heat are all examples. (Ellabban *et al*., 2014). In contrast to fossil fuels, which are depleted significantly faster than they are regenerated, renewable energy is rapidly replenished, although the majority of renewable energy sources are long-term.

Electricity generation, air and water heating/cooling, transportation, and rural (off-grid) energy services are all common uses of renewable energy (Murdock *et al*., 2020). Renewable energy businesses employ around 10 million people worldwide, with solar photovoltaic being the largest renewable employer (Ferroukhi *et al*., 2020). Renewable energy systems are fast becoming more efficient and affordable, and their percentage of overall energy consumption is rising, (Chan-Olmsted *et al*, 2019), with renewable energy accounting for the vast majority of newly added power capacity worldwide (Zhongming *et al*., 2019). Photovoltaic solar or onshore winds are the cheapest new-build electricity sources in most countries.

The photovoltaic (PV) system uses organized semiconductor materials to gather and convert solar radiation into electricity. PV cells, on the other hand, were harmed by their high cost and low absorption. As a result, to increase the absorption of PV active materials, a light restricting technique is necessary (Abdel-Latif *et al*., 2021). A thermophotovoltaic (TPV) system can also be used as a power source. The first TPV is invented by Dr. Henry Colm at Massachusetts Institute of Technology's (MIT) Lincoln Laboratory six decades ago for industrial waste repossession TPV technology is attract greater attention today (Rashid *et al*., 2020).

Thermophotovoltaic system is the system that crop electromagnetic field and alter it into electrical energy. Thermophotovoltaic system providing more opportunities to generate electricity since it has high ability to capturing several amount of energy which is maximum according to theoretical efficiency and it is also tailored to several temperature ranges. TPV system has three fundamental parts such as, heat source, emitter and TPV cell. Heat source is the source of photon such as solar burning fossil and waste energies. Emitter is the engineered devices which are convert the photon from heat source to thermal radiation. The TPV cell collects the emitted thermal radiation, which can generate electron-hole pairs and thus photocurrent. The conversion of electromagnetic energy to electrical power happens only when the photon energy is higher than the energy band gap of the TPV cell (Woolf *et al.*, 2018).

The basic problem for TPV systems are low conversion efficiency and power generation. In order to improve power generation, near-field thermal radiation has been proposed by bringing the emitter and TPV cells close to each other. However, it is still difficult to realize the nano-scale TPV systems in the near future. Also, to improve the conversion efficiency, a TPV emitter have highest possible emittance in a range of cut of wavelength that fits a specific TPV cell and the lowest possible emittance out of cut off wavelength. This is due to TPV cell can generate electron hole pairs and produce electricity for the photon with energy above the band gap but, below the gap generate electron hole pairs with insufficient energy that increase thermal energy TPV cell. Generally the high emittance in the range of targeted cut off wave length is help to maximize power generation and conversion efficiency of TPV system. Whereas, low emittance below cut off wave length is decrease thermal degradation of TPV cell (Gu *et al*, 2015).

As stated before the efficiency of the TPV system is depend on emitter which can be controlled by both the choice of material and the emitter design. For construct TPV emitter efficiency, temperature resistance, and how their cutoff wavelength match to the TPV cell was prerequisite. Emitter is designed from different material such as Polycrystalline silicon carbide, Tungsten, Rare-earth oxides, Photonic crystals, and metamaterials. However for increase the efficiency of emitter, power generation and performance of TPV cell metamaterials is more selective (Sakakibara *et al*, 2019).

Metamaterials (MM) are man-made materials with unique features such as repeating patterns on microscopic sizes that do not exist in nature. They're made up of numerous components comprised of composite materials including metals and polymers. The materials are often organized in repeating patterns on sizes smaller than the wavelengths of the phenomena they affect. The characteristics of MM are derived from their uniquely developed structures, not from the qualities of the underlying materials. Their exact shape, geometry, size, orientation, and arrangement confer on them the ability to influence electromagnetic waves. They are used for a variety of purposes, one of which is as an absorber.

Landy (2008) proposed the first MM absorber, which is a narrow band absorber based on metal–insulator–metal (MIM) (Landy *et al*, 2008). Many academics have constructed many types of MM absorbers after Landy for attaining single band or multiband absorption, but most scholars have recently shown a strong interest in ultraband absorption. Scholars primarily postulated and demonstrated that metal nanostructures extended the absorber's absorption spectrum. According to Kirchhoff law, the absorber produced from metal nanostructure is employed as a broadband absorber that is used as a metamaterial emitter. To improve TPV performance, MM emitters are often built with diverse symmetry shapes such as disk, square, crosses, pyramid, nanowire, cone, and nanoparticle (Maremi *et al*., 2018).

1.2. Statement of the Problem

A thermophotovoltaic energy conversion system is a new technology that has the potential to provide certain distinct benefits. The usage of a TPV cell is an ingenious technique to harness solar energy or recycle waste heat from industrial operations such as nuclear power generation (Teofilo *et al*., 2008), concentrated solar power (CSP) waste heat ((Seyf *et al*., 2016)), as well as other industrial activities using high temperatures. TPV System convert energy in a static manner, devices made comprised of heat source, thermal emitter, and a thermal receiver with no moving parts TPV cells. A thermal emitter is linked to a TPV cell in a TPV system, which is a static energy conversion device with no moving parts, whereas a heat source is a source of photons. The TPV cell is in charge of converting the heat radiation from the emitter into electricity. The use of an emitter with an output spectrum tailored to the TPV cell's response (rather than blackbody radiation) is a significant advancement in this technology. Furthermore, depending on the temperature of operation, a TPV system's efficiency might reach as high as

80%, according to Carnot efficiency. Because of these characteristics, TPV systems might be a viable option for energy collecting. The TPV emitter, on the other hand, is critical to conversion.

Previously, different scholars designed metamaterial emitters to increase the efficiency of the TPV system. Using COMSOL Multiphysics numerical analysis, Jiang *et al*. (2019) proposed a wavelength-selective TPV emitter based on a multilayer ring with an Al_2O_3 spacer over a tungsten film. The Multilayer of Jiang *et al*. (2019) achieves a spectral efficiency of about 58.2% and 72% at 1000 K and 1200 K, respectively, for the EQE of InGaAsSb. Maremi *et al.* (2018) also designed a multilayered metamaterial emitter based on a nano-ring structure of an AlN spacer over a tungsten film by using COMSOL Multiphysics numerical analysis. This emitter achieved 59% and 71.6% spectral efficiency at 1000 K and 1200 K respectively, for EQE of InGaAs. Many researchers have designed metamaterial emitters with various geometries to improve the efficiency and power conversion of TPV systems. However, even now, the emissivity in the range of the cutoff wavelength is not unity and decreases to zero above the cutoff wavelength. This work proposes to increasing emissivity near to unity in the cutoff wavelength range and decreasing to zero outside of the cutoff wavelength range for high spectral efficiency and TPV performance.

1.3. Significance of the Study

A significant aspect from a numerical study of high spectral efficiency and high temperature energy harvesting metamaterial emitters to improve TPV performance is to reduce the emission spectrum band gap of InGaAs that does not convert to electricity by minimizing it to zero. The emission spectrum below band gap energy is unnecessary absorption (emission) that invariably leads to raising the temperature of the cell and thus reducing its conversion efficiency. Furthermore, tailoring the excessively energetic part of the spectrum to a range of energies only slightly above the cell's band gap will reduce thermalization losses and thus improve cell conversion efficiency even more. Also, upgrade the emission spectrum in the range of cutoff wavelength (above the InGaAs band gap) that is converted to electricity by maximizing to one. The emission spectrum above the band gap (below cutoff wavelength) is necessary absorption (emission), which is matched to the TPV cell and fully converted to electricity. This leads to increased power generation and conversion efficiency, which provides high electric power that can be used for different purposes.

1.4. Objective

1.4.1. General Objective

The main objective of this work is to study thermophotovoltaic emitter based on metamaterial to improve spectral efficiency and efficiency of thermophotovoltaic system.

1.4.2. Specific Objective

The specific objectives are:

- ✓ To increase emissivity near to unity below cutoff wave length and reduce emissivity to zero above cutoff wavelength,
- ✓ To obtain a broad band and wide-angle selective emitter
- ✓ To optimize parameters to enhance the spectral efficiency of the emitter for bandgap of Indium Gallium Arsenide (InGaAs) and the efficiency of the thermophotovoltaic system.

1.5. Organization of the thesis

The current research was divided into five chapters. The first chapter provides a basic introduction to the TPV system, background of study, the objective of study, problem of statement, and significance of study. The second chapter illustrates the literature review on TPV, electromagnetic waves, the principle of TPV, components of TPV, challenges of TPV and their solutions, and the application of the TPV system. The third chapter describes the methodology used: materials, numerical simulation, and physical absorption. The fourth chapter explains and discusses the study's findings, such as the effect of different geometry factors, angular emissivity, energy distribution, performance of the TPV emitter, and performance of the suggested TPV with different metals and dielectrics. Chapter five illustrates the conclusion of the study and makes a recommendation.

2. Literature Review

2.1. Electromagnetic wave

To understand how to improve the selective emitter, one must first understand electromagnetic radiation and how it interacts with the material. In order to know how light interacts with a substance, it is vital to understand the dual nature of light. Photons, the quantized form of light, act as both particles and waves. Light was once supposed to be made up of minuscule particles, according to experts. This was not the case, as Thomas Young's single slit experiment proved (Jeffery, 2001). In a laser experiment, Thomas Young proved that the diffraction pattern looked more like the constructive and destructive interference patterns that waves create while traveling through a gap. When a second slit was inserted, the old pattern returned, but each maximum was further divided by interference fringes.

This evidence of wavelike activity was bolstered by Maxwell's work on characterizing the behavior of electromagnetic waves. By merging and changing Ampere's (Equation 1), Gauss' (Equation 2, Equation 3), and Faraday's (Equation 4, Equation 5), Maxwell created a generalized set of equations that may express electric and magnetic fields in space and matter (Equation 4). Using these equations, he obtained a formula for the velocity of an electromagnetic wave (Equation 5). When he used the data to calculate the velocity, he realized that it was the same as the known speed of light. Maxwell concluded as a result that light, or more properly photons, must be electromagnetic waves (Jeffery, 2001).

$$\nabla \times B = \mu_0 \left(J + \varepsilon_0 \frac{\partial E}{\partial t} \right) \tag{1}$$

$$\nabla . E = \frac{\rho}{\varepsilon_0} \tag{2}$$

$$\nabla . B = 0 \tag{3}$$

$$\nabla \times E = -\frac{\partial B}{\partial t} \tag{4}$$

$$\mathrm{v} = \frac{1}{\sqrt{\mu_0 \epsilon_0}} = c \tag{5}$$

where, B is magnetic field strength, E is electric field strength, J is current density, μ_0 is free space permeability, ε_0 is free space permittivity, c is of light , and v is velocity of electromagnetic wave.

The quantized, particle-like properties of light have remained a mystery despite accumulating evidence that it behaves like a wave. To match the amount of radiation created by a blackbody on a regular basis, it was necessary to use a quantized particle with a limited amount of energy. For extremely long wavelengths, the Rayleigh-Jeans law functioned well, but it was far from complete (Branson, 2013). At lower radiation wavelengths, early models based on classical physics principles failed. Willem Wien's exponential-based model, Equation 6, got him closer to a solution, but it required specifying arbitrary constants a and b to fit the shorter wavelength experimental data (Jeffery, 2001).

$$u_{Wein}(\lambda, T) = b\lambda^{-5}e^{-a/\lambda T} \tag{6}$$

where λ is the wavelength, T is the blackbody temperature in Kelvins, u is the energy density, and a and b are constants in this equation. Even with properly established variables, his equation diverged significantly from the data in the long wavelengths. After a better approximation, Wien was able to identify an inverse link between the wavelength of the peak emission and the temperature of the emitting blackbody. As a consequence, the Wien displacement law Equation (7) was computed.

$$\lambda_{max} = \frac{b}{T} \tag{7}$$

where λ is the peak wavelength, T is the blackbody temperature and b is a constant equal to $2.897 \times 10^{-3}\ mK$ (Jeffery, 2001). As will be shown later, this rule was frequently used to match the selective emitters provided in this thesis to a suitable blackbody.

Until Einstein went beyond classical physics to describe light, the whole blackbody spectrum remained unknown. Planck assumed that a blackbody could only absorb light of certain energies, but Einstein's statistical study of the system revealed that those were the only energy levels that existed. To put it another way, light is quantized into discrete energy levels proportional to its frequency, as indicated in Equation (8).

$$\mathrm{E} = hf \qquad (8)$$

Heinrich Hertz's discovery of the photoelectric effect in 1887 (Jeffery, 2001) confirmed this idea and enabled the measurement of Planck's constant. Hertz was the first to notice that when light strikes a metal, an electric current is generated. Robert Millikan expanded on this conclusion in the early 1900s by doing more precise measurements under vacuum. At the time, the most precise measurement of Planck's constant was made by measuring current generated by a range of light wavelengths on a newly cut metal surface in a vacuum (Millikan, 1916). Using electromagnets to align metal samples in an evacuated glass tube, he was able to scrape a pristine, scarcely contaminated surface that was subsequently bombarded with light of a certain frequency. Planck's law was written in its entirety.

Heinrich Hertz's discovery of the photoelectric effect in 1887 (Jeffery, 2001) confirmed this idea and enabled the measurement of Planck's constant. Hertz was the first to notice that when light strikes a metal, an electric current is generated. Robert Millikan expanded on this conclusion in the early 1900s by doing more precise measurements under vacuum. At the time, the most precise measurement of Planck's constant was made by measuring current generated by a range of light wavelengths on a newly cut metal surface in a vacuum (Millikan, 1916). Using electromagnets to align metal samples in an evacuated glass tube, he was able to scrape a pristine, scarcely contaminated surface that was subsequently bombarded with light of a certain frequency. The discrete property of photons was used to derive the entire form of Planck's law, as seen in Equation (9)

$$\mathrm{E}_{\lambda}(\lambda, T) = \frac{2hc^2}{\lambda^5}\frac{1}{e^{\frac{hc}{\lambda KT}}-1} \qquad (9)$$

where, E denotes spectral radiance, K denotes the Boltzmann constant, h denotes Planck's constant, and c is the medium's speed of light (Jeffery, 2001). Both characteristics of light must be present for a thermophotovoltaic system to perform. Individual electrons are promoted to the conduction band by the quantized photons in the TPV diode, resulting in the creation of electricity.

Sophisticated electromagnetic radiation manipulation has also facilitated the production of perfect absorbers and emitters, which have various applications in photodetector, photovoltaic, and thermophotovoltaic enhancement. Electromagnetic waves interact with materials, allowing for the creation of novel devices such as PV and TPV cells, photodiodes, and more. Electromagnetic waves can travel through vacuum, which has permittivity (ε_0) and permeability (μ_0). When an electromagnetic wave penetrates into a medium other than vacuum, its propagation properties vary according to the constituent atoms, electrons, and other particles present inside the medium. Atoms and electrons, for example, may substantially affect the behavior of light inside a medium by reducing the phase velocity (Fowles, 1989).

2.2. Principles of Thermophovoltaic system

TPV systems convert incoming electromagnetic radiation into direct current (DC) electrical power in the same manner as standard photovoltaic cells do. The poor absorption of PV systems is attributable to a number of causes. Photons from the source make direct contact with the PV cell, which is the primary and most essential reason. Both photons (photons below and above the band gap) can enter the cell, causing thermalization loss, the system's deadliest adversary. Second, photovoltaic systems exclusively use photons from the sun or solar system as a source of energy. As a result, during overcast and wet days, the system suffers from a shortage of photons. It is, in general, a system that is impacted (Oelker *et al*., 2019).

Because of the tailored radiation source and spectrum that distinguishes TPV from regular PV solar cells; the TPV system has a higher absorption than ordinary PV. The TPV cell in a TPV system employs a hot thermal emitter as its energy source, allowing it to work considerably farther into the infrared. The photocurrent production by photons with energy outside the electronic band gap is required for TPV's thermal-to-electricity conversion (Fleming *et a*l, 2005). TPV works on the same concept as PV in that it uses a p-n junction to absorb optical light, produce and separate electron/hole pairs, and then convert that energy into electricity.

However, materials used in TPV cells often have a significantly lower band gap than materials used in solar PV cells. TPV cells using materials such as GaSb (Woolf *et al*, 2018), InGaAsSb, AlGaAsSb, InAsSb, InGaSb, InGaAs, and InAsSbP (Deng *et al*, 2014; Nguyen-Huu *et al*, 2016; Maremi *et al*., 2018; Omair *et al*., 2019). The photovoltaic effect is explained by the relationship between the blackbody emission law (Wien's law) and the photovoltaic effect, which explains why TPV cells are frequently made with materials with band gaps between 0.5eV (2.4797 µm) and 0.8eV (1.5498 µm). Because of its quietness, pollution-free nature, portability, low maintenance costs, and adaptability, thermophotovoltaic systems have a wide range of applications. Nuclear generators for space applications, hybrid electric cars, industrial and domestic power sources, waste heat recovery, solar thermophotovoltaic systems, and portable electric generators are all examples of viable thermophotovoltaic systems.

2.3. Component of Thermophovoltaic

To create and improve a TPV system, understanding the primary components of a TPV device and how they interact is obligatory. The basic components of a TPV system are shown in the diagram below. The essential components of a TPV system are depicted in the diagram: a heat source, a thermal emitter, and a thermophotovoltaic cell.

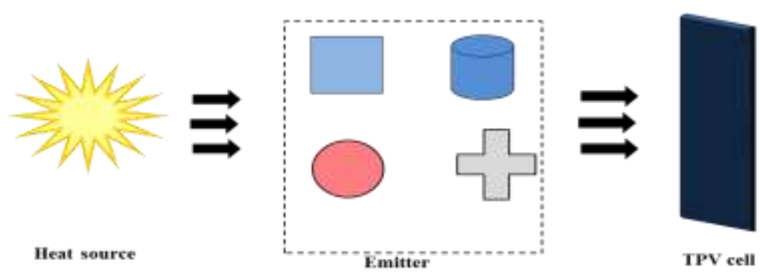

Figure 1: Basic schematic diagram of a TPV system

2.3.1. Heat source

The source of photons that function at a high temperature is referred to as the heat source. Chemical fuel, sunshine, radioactive isotopes (ß-photons), and flame combustion are some of these sources. Radiation transports heat energy from the heat source to the selected emitter. Waste heat from the industrial sector, particularly from iron and steel operations, has temperature levels that are acceptable for TPV systems. This heat source has a blackbody emission spectrum by definition. To increase cell efficiency, these emission spectra can be modified to minimize the energy in the long-wavelength tail below the TPV band gap (Pfiester, 2015).

2.3.2. Emitter

The emitter is a component of a TPV system that transforms heat from a heat source into thermal emission, which is subsequently emitted to the TPV cell. Although it may appear that a heat source should be sufficient to generate an emission spectrum, heat can also be carried through convection or conduction. Any heat created would be futile since only incident photons generate power. The habit of emitting permits the energy emitted by the source to be used more efficiently. The emitter also averages the photon flow to the TPV diode, resulting in a more steady and continuous current on the cell. Among the components of a TPV cell, the emitter is the most easily adjustable, as it controls the amount of heat radiation emitted (Sakakibara et al, 2019).

An emitter can be built in a variety of ways, each having its own geometric arrangement and materials. Additionally, while improving an emitter's optical performance is the primary aim of development, the best emitter for practical use is not always the best emitter with the best optical performance. Optical performance, large-area scalability, long-term high-temperature stability, simplicity of integration into the TPV system, and cheap cost are all recommended as a consequence (Sakakibara *et al*, 2019)

i. Optical performance

From all perspectives, a skilled optical performer preferentially emits in-band photons and suppresses out-of-band photons. Photon emission as a function of angle and photon energy is described by optical performance, with two separate regimes for the latter: in-band photons with energy larger than the TPV cell band gap and out-of-band photons with energy less than the TPV cell band gap. Spectral control refers to the methods used to enable preferred in-band emission. Some spectrum control schemes are more suited to wide-band emission, while others are better suited to narrow-band emission. In this case, the emitted photons have a larger energy than the PV cell's band gap (Sakakibara *et al*, 2019).

At any angle, a true emitter emits both in-band and out-of-band photons, but a TPV cell can only generate energy from in-band photons. As a result, the following problems develop: When out-of-band photons reach the TPV cell, they overheat it and impair its efficiency; when out-of-band photons are emitted but not recovered, the heat-to-radiation efficiency and emitter temperature both decrease (Sakakibara *et al*, 2019).

The spectrum emission can be regulated in two ways, as stated above for high optical performance gained by creating selective emitters. The first is to enhance in-band emission while suppressing out-of-band emission by using selective emitters. The alternative option is to utilize cold side filters or reflectors (CSFR) in front of (front side filter) or behind (back surface reflector) the TPV cell to reflect out-of-band photons back to the emitter, which is referred to as photon recycling. Combining both technologies, such as a selective emitter plus a filter or reflector, or possibly all three, is theoretically possible (Sakakibara *et al*, 2019).

ii. Ability to scale to large areas

Because the power emitted per unit area is the basic constraint for emitters, increasing the emitter area is one approach to increase the absolute radiated power (its macroscopic exterior dimensions). In terms of actual application, large-area substrates must be accessible, and manufacturing procedures must be able to support large-area samples (Sakakibara *et al*., 2019).

iii. Long term High-Temperature Stability

The optical performance of a TPV emitter must be maintained at high temperatures for long periods of time, either continuously or during several thermal cycles. At high temperatures, however, atoms' kinetic energy rises and they diffuse more easily, potentially resulting in a variety of thermodynamic consequences. Selecting materials with proven high-temperature qualities, alloying to encourage a solute drag effect, and changing the shape of a structure to adjust diffusion rate are some of the ways for increasing high-temperature stability (Stelmakh, 2017).

iv. Ease of Integration within the TPV System

The emitter's design choices can pose a number of issues for its integration into the TPV system, including physically joining the emitter and heat source for thermal contact and packaging the system for use in a vacuum or inert gas environment (Sakakibara *et al*., 2019).

v. Costs

The total cost of emitter manufacturing is determined by raw material costs, fabrication costs, and system integration costs. Many emitters, in particular, require relatively scarce elements like hafnium and rare earth metals. Fabrication costs may rise as the number of processing stages or the complexity of fabrication methods rises.

2.3.2.1. Types of emitter

Depending on the range of wavelength of the emissivity, emitters are classified into Broadband and Selective emitters.

1. Broadband emitter

The spectrum of a broadband emitter, as the name indicates, encompasses a wide range of wavelengths. Because their spectrum is equivalent to that of a black body are referred described as such. However, their emissivity is not nearly equal to unity at all wavelengths. Broadband emitters frequently employ bulk materials such as silicon carbide (Chubb, 2007). Although the existence of many photons with energies greater than the band gap energy can improve thermalization, the wide frequency range allows more power to be passed on to the TPV diode, resulting in a higher power output (Chubb, 2007).

Thermalization should be avoided in general since it causes a drop in output voltage (Hirst *et al*, 2011). When photons with energies substantially higher than the band gap energy are absorbed, the absorbing electron is promoted to a higher state in the conduction band. The electrons, on the other hand, cool at the conduction band edge since the lowest energy state is their preferred condition. The creation of phonons occurs when excess energy is passed to the lattice (Hirst *et al*, 2011). In the cell, an increase in phonons, or lattice vibrations, results in more entropy rather than useable electrical energy (Würfel *et al*, 2016). Recent work in hot carrier solar cells tries to make advantage of carriers in high-energy states before thermalization, although traditional methods try to limit its effect (Würfel *et al*, 2016)

2. Selective emitter

Is the emitter that is becoming increasingly common as a component of current TPV systems since it only emits a small range of wavelengths, resulting in improved conversion efficiencies. Regardless of the photons or heat energy impinging on it, the selective emitter will continue to radiate its distinctive spectrum. This is beneficial for a TPV system because the emitter may be chosen based on its ability to emit around the band gap of the diode, increasing efficiency. On the other side, the narrow frequency range produces less power. To get the most out of a selective emitter, you need to strike a balance between efficiency and power (Sakakibara *et al*, 2019).

2.3.2.2. Material used for emitter

The majority of work on TPV emitters has concentrated on attaining strong optical performance, with little attention paid to the issues of integrating the emitter into and managing a TPV system. Polycrystalline silicon carbide, rare-earth oxides, transition elements, Photonic crystals, and metamaterials are used to make the emitter.

1. Poly crystal Silicon carbide

Polycrystalline silicon carbide is the most common emitter for burner TPVs (SiC). Up to 1700 degrees Celsius, SiC is thermally stable. SiC is only used in TPV cells with a narrower band gap since it emits a lot of energy in the long wavelength region. In a TPV cell with a large band gap, the radiation is not converted into electrical energy. Long wavelengths can be reflected back to the emitter using non-absorbing selective filters in front of the TPV or mirrors on the rear side of the TPV, recycling the unconverted energy. Polycrystalline SiC is also a low-cost material to manufacture (Bitnar, 2003).

2. Rare Earth

The absorption and emission spectra of lanthanides, or rare earth metals, have been revealed to be unique. Rare earth oxides have now been shown to be a viable source of radiation for TPV and other uses as a result of this finding. Oxides are the most often used rare earth compound, especially for high temperature applications, since they are the most thermodynamically stable form of rare earth. Incorporating rare earth ions into host materials has also aroused interest as a way to combine the spectrum performance of lanthanides with the excellent thermal performance of other ceramics and crystals (Pfiester, 2015).

A rare earth metal's photon emission is caused by a high-energy electron descending to a lower-energy state. Because of the lanthanides' unique atomic structure, emission in the wavelengths characteristic to each metal is maintained even when a lanthanide atom is bound to another molecule. Rare earth oxides are attractive for high-temperature applications since because of their thermodynamic stability. Rare-earth oxides such as ytterbium oxide (Yb_2O_3) and erbium oxide (Er_2O_3) commonly used selective emitters for TPVs. These oxides emit a narrow band of wavelengths in the near-infrared region, allowing the tailoring of the emission spectra to better fit the absorbance characteristics of a particular TPV cell. Yb_2O_3 are can be used as selective emitter for Si, GaSb or InGaAs TPV cell. However, the slight mismatch between the emission peaks and band gap of the absorber results in a significant loss of efficiency (Jin *et al*., 2016).

3. Transition Element

From transition metal Tungsten is the most common choice. It has higher emissivity in the visible and near-IR range of 0.45 to 0.47 and a low emissivity of 0.1 to 0.2 in the IR region (Lambert *et al*., 2019). Based on this tungsten is only used for selective emitter it does not applicable for broad band emitter. On the hand in the near-infrared, TPV emitters made of Co or Ni-doped refractory oxides like Al_2O_3 and MgO.

4. Photonic crystal

Photonic crystals (PhCs) provide a more engineerable selective emitter than what is naturally available. A photonic crystal is a one-, two-, or three-dimensional arrangement of various materials. The number of planes of photonic response created is determined by the repetition dimensions, whilst the size of the repeated geometries affects the wavelength. Metallic photonic crystals made of tungsten or tantalum (Rinnerbauer *et al*., 2012.) Show potential as high-temperature emitters, although they often necessitate particular packaging, such as maintaining an inert environment. The low energy photons that impact the TPV diode are reduced by the sharp turn-on frequency caused by these devices (Rinnerbauer *et al*., 2012.) Many of them, however, maintain a strong emissivity of high-energy photons at frequencies higher than the turn-on frequency (Rinnerbauer *et al*., 2012.). The relaxing of these high-energy photons can result in parasitic device heating and lower conversion efficiency. Furthermore, difficulties in fabricating tungsten nanostructures may limit the range of possible uses.

Photonic crystals characteristic spectra are not simply determined by the atomic structure of their constituent materials. Rather, complicated optical phenomena cause selective emission. If the wavelength is on the order of the layer thickness, light impinge on a multilayer film consisting of materials with differing permittivities causes reflection and interference between the layers. In the wave vector diagram, this interference leads in forbidden photon momentum vectors, is appear as a photonic band gap. Bloch wave vectors that lie in the Brillouin zone anticipate the permitted states. Because the concept is easily applied to two and three dimensional structures, PhC behavior is frequently addressed in terms of the photonic band gap. (Pfiester, 2015)

Surface plasmon resonance (Robertson *et al*., 1999; Martin-Moreno *et al*., 2001) Resonant cavity amplification (Ryu *et al*., 2003), Wood's anomaly (Chen *et al*., 2007), Bragg reflection (Richel *et al*., 2000) and modification of the photonic density of states (Lin *et al*., 2000) are just a few of the distinctive phenomena that can be elicited by manipulating the PhC design. Depending on the design in use, the emission mode employed varies. Multiple resonant modes arise at various wavelengths in some situations, resulting in multiple emission peaks in the final spectrum (Babiker *et al*., 2014). The generated resonant modes can also be utilized to improve the performance of the gadget. When employing polar materials, surface phonon polariton coupling, for example, can dramatically improve near-field energy transmission in the IR. The use of PhC structures, however, reveals a trade-off between near-field amplification and spectral selectivity (Rodriguez *et al*., 2011).

5. Metamaterial

A metamaterial is a substance that has been manufactured to have a property that is not found in naturally occurring materials. They are made up of a number of parts made up of composite materials such as metals and polymers. The materials are usually arranged in patterns smaller in size than the wavelengths of the phenomena they influence. Metamaterials receive their attributes from their newly constructed structures, not from the parent materials' properties. Backward propagation, negative refraction, diffraction-limit breaking imaging, cloaking, and other non-natural electromagnetic phenomena are some of them. Their smart capabilities are derived from their exact structure, geometry, size, orientation, and arrangement, which enable them to control electromagnetic waves by blocking, absorbing, amplifying, or bending waves to provide benefits not possible with regular materials (Bermel *et al*., 2011).

MM are used for antenna, absorber, super lens, cloaks, photonics or opto-electronics, and solar cells. The MM that used as absorber is used as emitter according to Kirchhoff law. Kirchhoff's law of thermal radiation refers at specific wavelength-specific radiative the emission and absorption by a material body in thermodynamic equilibrium (Kirchhoff, 1978). Therefore better absorber is better emitter at specific wavelength. MM emitter is designed as Metal Dielectric Metal (MDM) by different geometry for TPV system to increase the efficiency and performane of TPV system. MM emitter is more selective for TPV system because of its unique property to control electromagnetic wave in selected wavelength.

2.3.3 Thermophotovoltaic cell

Photon energy is converted into electricity via a thermophotovoltaic (TPV) cell, which is a semiconductor. The band gap energy is the minimum energy required to remove an electron from a semiconductor. The energy for TPV cells comes from photons, which are tiny packets of electromagnetic radiation emitted by the emitter. When photons with a higher energy than the band gap impact the TPV cell, electrons absorb the energy and start moving, creating electricity. A photon that reaches a TPV cell below the band gap, on the other hand, absorbs as thermal energy (Abdul, et.al, 2020).

2.3.3.1 Material used for thermophotovoltaic cell

Exciting electrons with a lower band gap requires more photon energy, which is desired since it supplies the charges that allow current to flow. A small band gap, on the other hand, causes those charges to have a lower voltage. In materials with a high band gap, however, fewer photons have enough energy to form currents that transport electrons and holes, thereby limiting the amount of current that may be created. A big band gap, on the other hand, causes those charges to have a higher voltage. Because a low band gap semiconductor, such as germanium, gallium antimonide, Indium gallium arsenide, and Indium phosphide arsenide antimonide, produces more current with lower voltage and a high band gap semiconductor, produces less current with higher voltage, the material used as TPV cell is a low band gap semiconductor.

1. Germanium (Ge)

Another PV material that has been studied for use in TPV technology is germanium (Ge), which has band gap energy of 0.66eV. The 0.66eV band gap energy of germanium matches the radiation maximum of a blackbody radiator at 1540 K, according to a simple calculation. As a result, Ge may be suitable for use in TPV devices where the emitter temperature is typically less than 1800 K. Furthermore, when matched with Er_2O_3 emission, Ge TPV cells produce spectrum efficiencies that are significantly greater than those produced by matching a Si photocell with

Yb_2O_3 emission. Despite this, the effectiveness of Ge photocells is often lower than that of Si and GaSb TPV photocells. Ge cells are more expensive than Si cells; however they are still less expensive than III–V low bandgap cells like GaSb and GaInAsSb.

2. Gallium antimonide

Gallium antimonide is semiconducting compound of gallium and antimony which invented in 1989 by Victor Goldschimidt which is a semiconductor compound that belongs to the III-V family. It's one of the best semiconductor materials for TPV applications with temperatures ranging from 1300 to 1500 degrees Celsius. It has an excellent quantum efficiency of better than 90%, especially at IR wavelengths up to 1800 nm, due to its low bandgap energy, which is spectrally matched with the medium blackbody temperature. (Ni *et al*., 2016).

The early GaSb photovoltaic cell structure that is sensitive to the photons in the infrared region up to 1.8 µm. GaSb photocells are made using zinc vapor diffusion technology or epitaxial techniques such as liquid phase epitaxy (LPE) or metal–organic vapor phase epitaxy (MOVPE). Due to the ease of the manufacturing methodology, the GaSb cell generated by Zn diffusion method is currently preferred in a variety of TPV applications. GaSb solar cells have proven to be the most efficient semiconductors. However GaSb cells are toxic costive and is used in narrow wavelength (Gamel *et al*., 2021)

3. Indium gallium Arsenide

InGaAs is an III-V ternary semiconductor compound made up of indium and gallium group III elements, as well as the arsenide group V element. By varying the x composition in In_xGa_{1-x} As, the bandgap energy of InGaAs may be altered from 1.42 to 0.36 eV, corresponding to cut-off wavelengths ranging from 0.87 to 3.34 µm. With band gap energy of less than 0.74 eV, an InGaAs cell with a longer cutoff wavelength will improve mid-IR harvesting and thus boost output power. A reduced bandgap is achieved by using a lattice-mismatched InGaAs with greater indium content. Lattice-mismatched lower band gap is because of their wide range of applications, InGaAs cells have recently gotten a lot of press. In order to develop a lattice-mismatched InGaAs, the indium ratio was increased while the gallium ratio was decreased (Long *et al*., 2019).

When the bandgap of InGaAs is reduced the short circuit current increases, resulting in increased output power. However, fabricating a high-performance lattice-mismatched cell with a smaller bandgap on an InP substrate is a challenge. Auger recombination is more common in InGaAs with smaller band gaps, but Shockley-Read-Hall (SRH) recombination is more common in InGaAs with large defects caused by lattice mismatch epitaxy. Auger and SRH recombination both increase dark current and reduce device performance (Wanlass *et al*., 1999). The advantage of InGaAs cells is that they may achieve a cutoff wavelength of up to 2.6 µm. InGaAs is a semiconductor that can be used in electronics and photonics at room temperature.

4. Indium phosphide arsenide antimonide (InPAsSb)

Both OMVPE and LPE have been used to develop the InPAsSb quaternary alloy. It possesses a bandgap in the region of 0.3–0.55 eV when lattice-matched to InAs. The advantages of a TPV system with such a small band gap have not been thoroughly investigated. As a result, cells containing InPAsSb have not been optimized and do not yet perform competitively. The InPAsSb cell examined had the longest spectrum response of 4.3µm, with a maximum response of 3µm. While this material appears to be promising, it has yet to be developed. Due to an increase in Auger recombination, good IQE for long wavelengths is difficult to attain for this and other low-bandgap materials.

2.3.3.2. Efficiency of Thermophotovoltaic cell

The TPV cell efficiency is the product of four diode-physics processes, as given in the following equation:

$$\eta_{cell} = QEF_o \frac{V_{oc}}{E_g} FF \tag{10}$$

where, QE is quantum efficiency, F_o is excitation factor V_{oc} is open circuit voltage , E_g band gap energy and FF is fill factor. The quantum efficiency is a quantity that is proportional to the diffusion length and the surface recombination velocity. The quantum efficiency of the TPV cell increases its efficiency. A solar cell's quantum efficiency is the ratio of carriers caught to photons of a specific energy incident on the cell, which can be represented in terms of wavelength or energy. When all photons of a wavelength are absorbed and the resulting minority carriers are collected, the quantum efficiency is unity, but it is 0 for photons with energy below the band gap. IQE is always larger than the EQE in the visible spectrum. A low IQE indicates that the active layer of the solar cell is unable to make good use of the photons, most likely due to poor carrier collection efficiency. To measure the IQE, one first measures the EQE of the solar device, then measures its transmission and reflection, and combines these data to infer the IQE as below equation,

$$EQE = \frac{electron\,/_{sec}}{photon\,/_{sec}} = \frac{current\,/_{charge\ of\,1\ electron}}{total\ power\ of\ photon\,/_{energy\ of\ one\ phothon}} \quad (11)$$

$$IQE = \frac{electron\,/_{sec}}{absobed\ photon\,/_{sec}} = \frac{EQE}{1 - refelection - transmission} \quad (12)$$

As a result, both light absorption and charge collection affect the external quantum efficiency. After a photon has been absorbed and generated an electron-hole pair, these charges must be separated and collected at the junction. In a good material, charge recombination is avoided. As a result of charge recombination, the external quantum efficiency is lowered.

2.4. Challenges of Thermophotovoltaic system and solution

2.4.1 Spectral Mismatch to the Bandgap of TPV Cell Material

In theory, TPV cells are most efficient when the energy bandgap of the semiconductor is spectrally matched to the blackbody spectrum created by the heat source (Bauer, 2011). As a result, the material for TPV cells should be chosen based on the bandgap that corresponds to the spectrum. This is done to reduce optical loss due to spectrum mismatches and poor photon absorption by the TPV cell. Ten et al proved that that electricity conversion happens at photon wavelengths close to a materials cutoff of wavelength (Tan *et al*., 2014).

The emissivity of the practical radiator can be tuned to the TPV cell. Selective radiators can be designed to emit at a certain IR range. In brief, mismatching between the heat source spectrum and the cells bandgap is one of the major difficulties that results in reduced output energy and lower TPV system efficiency. As a result, aligning the blackbody spectrum to the appropriate range of TPV cell bandgap energy is critical for generating the most energy per unit area. The reflection and recycling of sub-bandgap photons in the radiator will significantly improve the TPV system's conversation efficiency (Gamel *et al*., 2021)

2.4.2. The Effect of Cell Temperature

To produce maximum light intensity, the TPV cells are normally operated at temperatures higher than 300 K and are situated near the heat radiator. Because the TPV cell is subjected to continual thermal radiation during operation, it may heat up to a point where it affects cell performance (Martín & Algora, 2004). Despite this, increasing the temperature of the TPV cell raises the energy due to a decrease in the bandgap (E_g) energy of the semiconductor material. With a lower E_g, more photons with a somewhat longer wavelength can be absorbed, resulting in more electron-hole pairs.

Several strategies can be used to solve the problem of elevated internal temperature in TPV cells. Aside from using a radiator and filter to prevent the cell from thermalization, active cooling systems including heat sinks, cycling coolant, and forced air coolant are often used in TPV prototypes (Fraas, 2014). Furthermore, using a transparent insulator layer or un-doped semiconductor layer to separate the cell from the radiator will aid to protect the TPV cell from the hot radiator. It would also lower the cell temperature by reducing heat transfer to the cell via conduction and convection.

2.4.3. Low Conversion Efficiency of Thermophotovoltaic Cell

The low conversion efficiency of TPV cells continues to be a major obstacle to developing a practical TPV system. In TPV, fundamental calculations may forecast optical-to-electrical conversion efficiencies, which is comparable to solar PV technology. In the real world, the entire TPV systems optical-to-electrical conversion efficiency is lower (Hitchcock *et al*., 1997). This is mostly owing to poor spectrum control from the generator to the TPV cell, which results in significant optical losses due to reflection and shading losses. The shading loss can be decreased by optimizing the metal coverage area on the cell active surface, while the reflection problem can be mitigated by using an ARC and a rear surface reflector. Electrical losses such as bulk and surface recombination, on the other hand, are influencing variables in cell conversion efficiency To maximize TPV cell efficiency both optical and electrical losses must be considered (Gamel *et al*., 2021).

Resistive losses, on the other hand, are proportional to the effectiveness of the metal contact, which allows for the smooth conveyance of photo generated carriers to the external circuit. Despite the importance of metal contact, the research of ohmic contact with semiconductor materials has received less attention. Aside from that, optimizing the TPV cell's ohmic superconductive metal interface would make high current density flow easier. This is possible by creating a transparent metamaterial metal with an ohmic work function (Gamel *et al*., 2021).

2.4.4. Distance between TPV cell and Emitter

Near field TPV system is built with a gap spacing of only a few nanometers to centimeters between the radiator and the TPV cell (Tian *et al*., 2018). The inverse square law (Tuley *et al*., 2012) shows that as the travel distance increases, the amount of power delivered falls significantly. Near-field coupling occurs at nanometer gap distances, resulting in Super-Planckian behavior. Because of its capacity to improve the amount of energy transferred into a TPV converter, near-field TPV has seen rapid growth in the theoretical, computational and experimental examination in recent years. Different materials and approaches are being researched in the near-field TPV, which is still in the early stages of modeling and simulation. Under low-radiation temperature (655 K), a near-field TPV system outperforms a far-field system for gap distances between 12 µm and 60 nm (Zhao *et al*., 2018).

2.4.5. Cost-Effectiveness of TPV Cell Commercialization

One of the most difficult aspects of TPV use is lowering the cost of commercialized TPV cells. Some of the TPV structures are made with costly growth techniques like MBE. In addition, to improve cell function, most TPV cells require front and back surface field layers. The collection of long and short photo generated carriers is aided by these layers (Gamel *et al*., 2019). As a result, costly epitaxial growth is used in the layer deposition process. Another issue that makes TPV manufacture inefficient is the lack of a lattice-matched TPV substrate. This is due to the high cost of producing thick TPV substrate, which makes fabricating thin substrate on a sub-micron scale a difficult task. As a result, using widely accessible and cost-effective substrates to grow TPV cells offers a significant answer to the high cost of TPV cell production. As a result, research into TPV materials that could potentially lower the cost of mass-scale TPV production is required.

2.5. Application of Thermophotovoltaic system

The TPV system has gotten a lot of attention because of its potential contribution as a cost-effective, efficient, and practical power system, as well as a source of clean energy. The use of TPV can be classified based on whether the thermal heat source is a chemical reaction or a nuclear fusion reaction. Solar heat, fuel combustion, nuclear sources, and waste heat are the several types of heat sources.

2.5.1. Solar TPV Systems (STPV)

The TPV cells convert the infrared photons into electricity using thermal radiation from these high-temperature radiators (Xuan *et al*., 2011). Zhou and colleagues (Zhou *et al*., 2016) conducted a thorough examination of TPV cells material in the STPV system. The STPV system in a hybrid system is attracting a lot of attention these days. Hussain et al. (Norton *et al*., 2017) investigated the performance of various hybrid STPV designs utilizing a solar-biomass/gas power production system. The hybrid STPV system may function at temperatures lower than 1273 K, allowing it to be used in additional applications such as a portable battery charger and a household microgenerator.

2.5.2. Combustion-Driven TPV Generators

Micro-, meso-, and macro-scale power supply applications can all benefit from a combustion-driven TPV system (Bitnar *et al*., 2013). Portable electric generators, combined heat and power (CHP), and hybrid electric cars are all examples of practical applications for combustion-driven TPV generators. In military applications, the portable TPV system was widely used to replace heavy batteries and noisy diesel-electric generators (Basu *et al*., 2007). Some scholars are developed a portable microgenerator but the findings suggested that additional work may be encouraged in order to improve conversion efficiency. This device is sometimes referred to as an off-grid generator because it is designed to deliver heat and energy to distant households during the winter and at night. The CHP-based TPV has been designed not just for residential usage, but also for larger scale applications such as central heating furnaces in large buildings and industrial furnaces (Fraas *et al*., 2003)

A TPV device converts the exhaust heat from a gas-powered engine to charge the batteries with enough power to accelerate and sustain a cruise speed in a hybrid electric vehicle (HEV). The demand for high efficiency is a fundamental concern for TPV generators in HEV. To attain high-performance HEVs, research efforts have been committed to future development for higher heat recovery and system efficiency. The design system uses a selective emitter and quantum well TPV cell that can theoretically provide 24.5 percent efficiency and 6 kW of electric power to replenish an electric city car's battery pack. However, more experimental research into the emitter-cell system is required.

2.5.3. Space Applications

In the future, high-efficiency TPV cells will be critical in space technologies (Bauer, 2011). Solar and nuclear generators are two viable power sources for powering a tiny spacecraft for an extended period of time (Schock & Kumar, 1995). A recent critical assessment of space power generation was done to compare the main competing technologies (Datas & Martí, 2017). The TPV system claims up to 40% efficiency, as well as the advantages of being lightweight, mechanically static, and producing direct energy from radiant heat in space power generation. In addition, as compared to other technologies, the TPV system generates a high power density per unit area, making it suited for medium electrical systems. With the use of radioisotope TPV generators and nuclear fission sources, the power density can be enhanced even more (Schock & Kumar, 1995). The thermal range for nuclear generators is typically 10 kW to MWs *(*Teofilo *et al.*, 2008) and these generators are currently being considered for use in future planetary colony missions (Datas & Martí, 2017)

2.5.4. Waste Heat Recovery (WHR)

According to a recent thermodynamic analysis of a TPV system used for industrial WHR, up to 7.31 percent of annual waste energy can be recovered. The potential of TPV heat recovery in the glass and steel manufacturing industries has become a popular research topic in recent years. Fraas et al. (Fraas *et al*., 2003) demonstrated a TPV cell with a power density output of 1.5 W/cm^2 per cell created from a hot glowing radiant tube burner (1548 K) in the steel sector.

2.5.5. Thermal Energy Storage System

Thermal energy storage applications are particularly interested in TPV devices. The thermal energy storage system is based on the use of ultra-high temperature phase change materials (PCM). The energy in this system is stored as latent heat and converted to electricity when needed using TPV cells. According to Datas et al. (Datas *et al*, 2016), a thermal storage system can achieve a thermal energy storage density of 1 MWh/m, which is 10–20 times higher than lead-acid batteries and 2–6 times higher than Li-ion batteries. Seyf and Henry (Seyf *et al*., 2016) created a model of a thermal energy storage system and identified the key design elements that influence the overall efficiency of the power cycle system.

3. Methodology

3.1. Material Selection

The structure was designed as a metal dielectric metal. The metamaterial structure model was made up of refractory metal Tungsten (W) at the top and bottom of layers and aluminum nitride (AlN) as a dielectric spacer. W has been used for high temperature applications due to a high melting point temperature of about 3722 K. AlN has a sufficient melting point temperature of about 2500 K and good oxidation resistance. Also, aluminium (Al) and molybdenum (Mo) are used in the place of tungsten (W) and aluminium oxide (Al_2O_3) and silicon dioxide (SiO2) are used in place of AlN for the comparison.

3.2. Numerical Simulation

Numerical simulation was performed by COMSOL Multiphysics software. COMSOL Multiphysics is simulation software that supports engineering, manufacturing, and scientific research organizations manage physics-based modeling by verifying and optimizing processes and devices. The platform enables users to create custom modeling workflows and facilitate data exchange between multiple models, including electromagnetics, heat transfer, structural mechanics, fluid flow, etc.

COMSOL Multiphysics provides geometry modeling tools such as solids, curves, surfaces, and Boolean operations, also it define the sequence of processes to obtain data for editing and parametric studies. The solution offers numerous functions such as virtual operations, CAD data import, predefined physics interfaces, automated and manual networking, 2D / 3D modeling and more. It also includes visualization and post-processing tools that enable researchers to view simulation data using interactive graphics, charts, and figures, and to export results in text, DAT, CSV, and Excel formats. Research professionals can also design custom modeling applications and share them with process operators, test labs, manufacturing departments, or customers.

Figure 3 shows a MM emitter made of tungsten and aluminum nitride (AlN) created with COMSOL Multiphysics software. A 3D spatial dimension was used for the working environment. The optical interface was utilized to compute electric and magnetic fields for our system, which has a wavelength that is comparable to or much smaller than the device being analyzed. To solve for time-harmonic electromagnetic field distributions, the EMWFD interface was chosen. The Wavelength Domain study was used to calculate the response of a model that has been subjected to harmonic excitation at one or more wavelengths. It was used to calculate the structure's transmission and reflection versus wavelength in electromagnetic wave propagation through the designed structure.

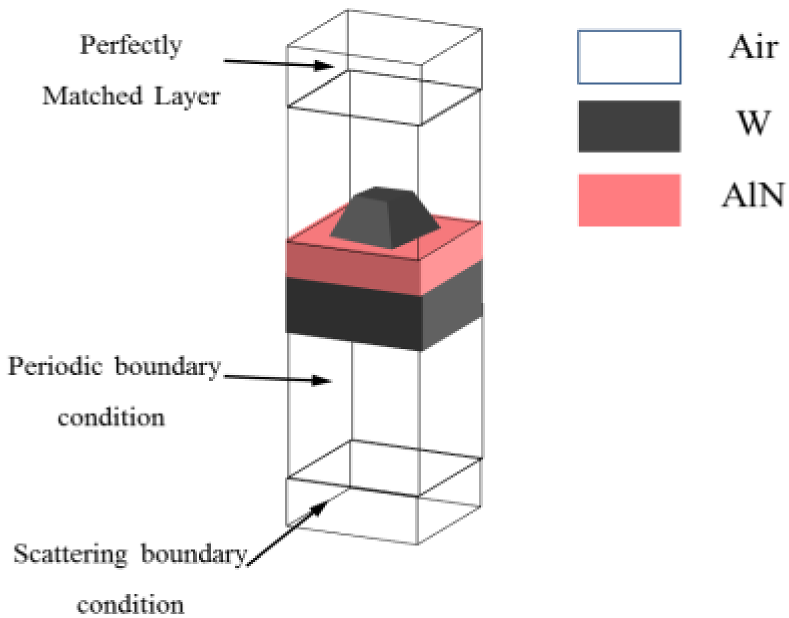

Figure 2: Design of metamaterial emitter for COMSOL Multiphysics simulation

The design parameters were w (width of unit cell), h_1 (top tungsten height), h_2 (dielectric thickness), h_3 (ground tungsten thickness), b_1 (base length of pyramid), b_2 (base width of pyramid), and with ratio bottom to top pyramid 0.5 are the design parameters. Air n = 1, W, and AlN optical material properties W and AlN have melting points of 3695 K and 2345 K, respectively. A nano-pyramid that starts with W and finishes with W, i.e. a metal-dielectric-metal structure, was constructed.

With the goal of reducing computational time, numerical simulation was performed on a single unit cell, as illustrated in Figure 3. COMSOL Multiphysics software was used to do three-dimensional electro-magnetic wave and wavelength domain research. To reduce reflection, perfectly matching layers were assigned to the top and bottom of the computational domains or along the z-axis during the numerical analysis. To account for an infinite flat surface on the emitter as well as oblique incidence, the periodic boundary condition was established at both the right and left borders. Through the working wavelength, electromagnetic waves or incident light on the emitter are believed to be perpendicular to the x-y plane. Through the working wavelength, the refractive index (optical characteristics) of W and AlN were taken from the software's default material list.

The following guidelines were an attempt to lay out some fundamental factors for constructing the suggested geometry: 3D, Optics, Wave optics, EMWFD, Add, Study, Wavelength domain, done. During simulation, a Perfectly Matched Layer (PML) is added on the top and bottom of the computational domains to minimize reflection. The layer of virtual domains surrounding the physical region of interest is subjected to sophisticated coordinate scaling by the Perfectly Matched Layer node. This layer absorbs all outgoing wave energy in frequency-domain problems when properly tuned, with no impedance mismatch at the boundary creating spurious reflections. A Perfectly Matched Layer was created by clicking Perfectly Matched Layer on the Definitions toolbar. Each simple connected PML area requires its own Perfectly Matched Layer node. That is, all PML domains must be in touch with each other in order to use the same Perfectly Matched Layer node. Otherwise, the PMLs will not function correctly.

The electromagnetic properties, such as Periodic Boundary Condition and Scattering Boundary Condition, are created by numerical simulation. The Periodic Boundary Condition establishes a pattern between the chosen limits. The Destination Selection sub node can be accessed via the context menu (right-click the parent node) or the Attributes menu on the Physics toolbar. The Scattering Boundary Condition is to make a boundary transparent to a scattered wave. For an incoming plane wave, the boundary condition is also transparent, which was created from the scattering boundary condition from the physics toolbar.

Port and scattering parameter

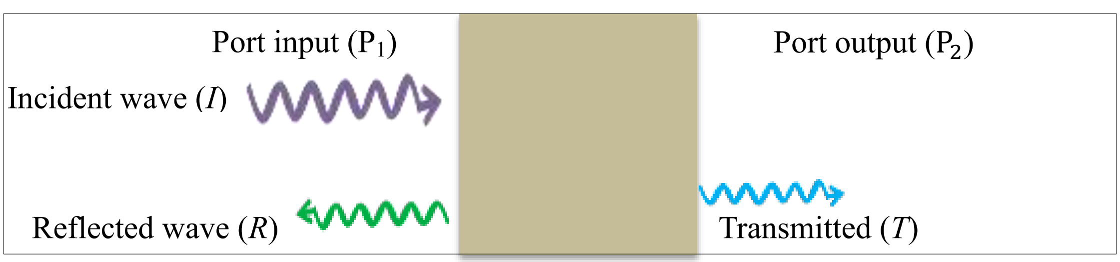

Figure 3: Showing port and scattering parameters. Port input (P_1) the left hand side, Port output (P_2) the right hand side. Incident wave (*I*) reflected wave (*R*), and transmitted wave (*T*)

Two ports were taken into account throughout the numerical analysis. The first port, which produced electromagnetic waves, was known as the "in-port," while the second port was known as the "out-port." When an electromagnetic wave is incident on a plane, it may be absorbed, reflected, or transmitted. The absorption is calculated as,

$$A = 1 - R - T = 1 - (s_{11})^2 - (s_{21})^2 \quad (13)$$

where, A is absorptivity, R is reflectivity T is transmittance , s_{11} is reflection coefficient and s_{21} is transmission coefficient . The transmittance of the W film is zero (T = 0) because the skin depth of the W film is less than 100 nm (Smith *et al.*, 2002), and a mid-infrared electromagnetic wave cannot travel through the W film. Therefore the absorption can be expressed as,

$$A = 1 - R = 1 - (s_{11})^2 \quad (14)$$

The absorptivity and emissivity derived by using Kirchhoff's law, which stipulates that the higher the absorptivity, the higher the emissivity. With the assumption of no transmittance, an objects emissivity is equal to its absorptivity for a given frequency, polarization, and direction:

$$\varepsilon(\lambda) = A(\lambda) = 1 - R = 1 - (s_{11})^2 \quad (15)$$

Substance must have minimal to no transmission and reflection of impinging light to function as a perfect absorber. When the materials impedance is equal to the impedance of open space, reflection is minimized. Permittivity (ε) and permeability (μ) are related to a materials impedance, z, and index of refraction, n, via Equations 16 and 17, implying that impedance is a function of and through Equation (18) (Smith *et al.*, 2002) .

$$\varepsilon = n/Z \quad (16)$$

$$\mu = nZ \quad (17)$$

$$z = \sqrt{\frac{\mu}{\varepsilon}} \quad (18)$$

The refractive index of a material is also related to the relative ε and μ through Equation 19,

$$n = \sqrt{\varepsilon_r \mu_r} \quad (19)$$

where the relative permittivity is

$$\varepsilon_r = \frac{\varepsilon}{\varepsilon_o} \tag{20}$$

and the relative permeability is

$$\mu_r = \frac{\mu}{\mu_o} \tag{21}$$

Scattering parameter describes the transmission and reflection of electromagnetic waves at ports. The impedance of material can be calculated from S-parameter as Equation (22) (Smith *et al*., 2002),

$$\boldsymbol{z} = \pm\sqrt{\frac{(1 + s_{11})^2 - s_{21}{}^2}{(1 - s_{11})^2 - s_{21}{}^2}}\, s_{21} \tag{22}$$

where, s_{11} reflected signal port is

$$s_{11} = \frac{R}{I} \tag{23}$$

where, s_{21} transmitted signal port is

$$s_{21} = \frac{T}{I} \tag{24}$$

Finally, the simulation findings were used to calculate the emissivity based on absorptivity. When creating a COMSOL model, there are a few things to keep in mind. Regularity, in particular, should be used as often as feasible because it will considerably minimize simulation run time.

3.3. Physical Mechanism of absorption

Absorbers must be heated by absorbing thermal energy from the source in order to operate MM as an emitter. Photons will be emitted in the intended emission spectrum when enough thermal energy is applied. There are various physical mechanisms that can increase the amount of spectrum absorbed or emitted. In this section, we will go over a few of the techniques that are used in the suggested emitter.

3.3.1. Surface plasmon polariton

When an incoming photon is associated with a Surface plasmon (SP), the result is a Surface plasmon polariton (SPP). SP is a collective excitation of electrons (electron density) at the dielectric-metal interface caused by the dielectric material's positive permittivity and the metal's negative permittivity behavior at optical frequency. Because of excitation of surface plasmon polariton (SPPs) on corrugated metal surfaces or stimulation of resonant modes restricted in sub wavelength metallic cavities, metals are commonly thought to be excellent reflectors. However, reflection fades away when they are structured on a wavelength scale, and improved absorption occurs with a crisp spectrum much narrower than that of a blackbody (Zhang *et al.*, 2011).

Once stimulated, the SPPs proceed in a parallel route along the metal-dielectric contact. The wavelengths of SPPs are much shorter than those of incoming photons. Their primordial life is brief, and they degenerate rapidly in a perpendicular direction over metal-dielectric contacts. The surface plasmon is formed by the collective excitation of electrons between tungsten and aluminum nitride, according to this study. When the aggregate excitation of photons together with the incoming electromagnetic wave enters through the port, SPPs are excited.

3.3.2. Magnetic Polariton

Magnetic polariton is the resonance of magnetic oscillation on a material surface in combination with incoming photons, which is mostly governed by the materials plasmonic properties and geometric parameters. When significant diamagnetism occurs, the material reaction resonantly boosts the total magnetic field, changing the actual component of the magnetic permeability to be negative. When photons collide, they produce an oscillating magnetic field, which causes current to flow in one direction in the MM and in the other way near the metal substrate's surface. Due to the existence of free charge on the metal substrate, there was a net flow of oscillating electric currents, resulting in induced magnetic fields. The diamagnetic response is brought about (Maremi *et al*., 2018). According to this study MP are exited due to the existence of free charge on the upper and bottom tungsten there is a net flow of current in dielectric that resulted in induced magnetic field.

4. Result and Discussion

Figure 4 shows the designed three-dimensional metamaterial emitter. The topmost layers were made up of a square lattice of P-periodic tungsten (W) arrays. W has been used in high-temperature applications due to its high melting point (3695 K). AlN has a good melting temperature (2345K) and, more importantly, oxidation resistance. A unit cell is designed with a W at the top, which has a pyramid structure and a periodic distance. A thin film of AlN was designed on top of a W film, which acted as a perfect reflector

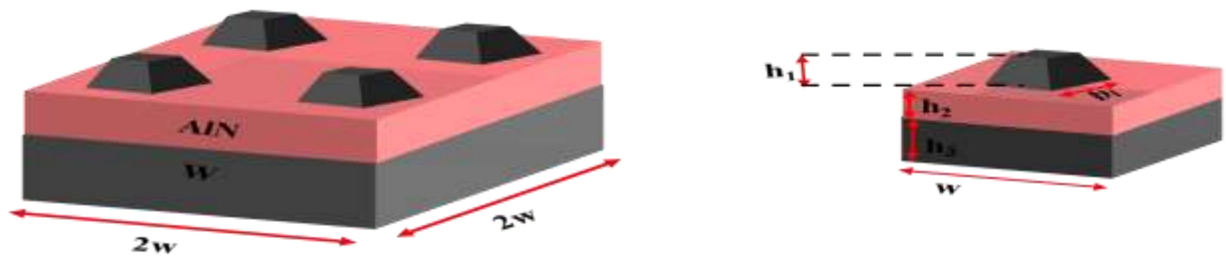

(a) **(b)**

Figure 4: (**a**) Schematic representation of the designed metamaterial structure (**b**) unit cell of the reported nano pyramid

The width of the unit cell was (w) and the W film thickness (h_3) at the bottom was fixed at 395 nm and 260 nm, respectively. On the other hand, parameters such as base length of pyramid (b_l), height of pyramid (h_1), and thickness of dielectric (h_2) were variable, as well as the ratio between top and bottom length of the pyramid was 0.5.

To prevent incoming light transmission, AlN was used as a spacer layer with a thickness of h_2. COMSOL Multiphysics generated an electromagnetic wave with a frequency of 300 THz from the in port to the constructed MM emitter. The results below were achieved after a lot of trial and error. The effect of varying parameters on the emissivity of the MM emitter was discussed in the following subtopics. Furthermore, the impact of polar and incident angle on emissivity, the performance of TPV, and the performance of a suggested TPV emitter with different dielectric and metal were discussed.

4.1. Effect of base length of pyramid

To control the effective permittivity and permeability of metamaterials, the geometry and arrangement of the design are the most noticeable. Metamaterial interacts with impinging electromagnetic waves due to current induction in the metallic periodic structure. The wave of the magnetic component travels perpendicular to the plane of pattern. The direction of the magnetic field creates a current in the conducting metal, as demonstrated by the right-hand rule that is taught in fundamental electricity and magnetism classes. This current generates a magnetic field, which can increase or cancel the wave impinging magnetic component. The apparent impact is a uniform decrease in effective permeability since the pattern is smaller than the wavelength of the targeted frequency. Because of interactions between the electric wave component and the induced electric field, the electric component of light may also create an induced magnetic field, which influences the permittivity of the material. Structures have also been built that combine these effects to vary the effective permittivity and permeability at the same time. The structure that manipulates both components of an electromagnetic wave at the same time exists in three dimensions based on how each component interacts with the planar metal patterning of an MM (Pfiester, 2015).

As a result, the periodic unit cell arrangement and the geometry of metamaterials were the sources of electromagnetic property. Change the characteristics of the W and AlN, such as base length of the pyramid, height of the pyramid, and thickness of the dielectric, to modify the electromagnetic properties. Figure 5 (a) and (b) showed the emissivity of the designed emitter when b_l was varied from 95 nm to 295 nm. As seen from the figure, the emissivity peak of the designed MM was shifted to the longer wavelength with a low value. When b_l was increased from 95 nm to 215 nm, the average emissivity before the cutoff wavelength (black dotted line) increased, whereas when b_l was increased from 215 nm to 295 nm, the average emissivity decreased. The graph demonstrated the emissivity of the designed emitter was increased after the cutoff wavelength when b_l was enlarged from 95 nm to 295 nm. At a small value of b_l, the emitter had a high value at a smaller wavelength and a low value at a high wavelength.

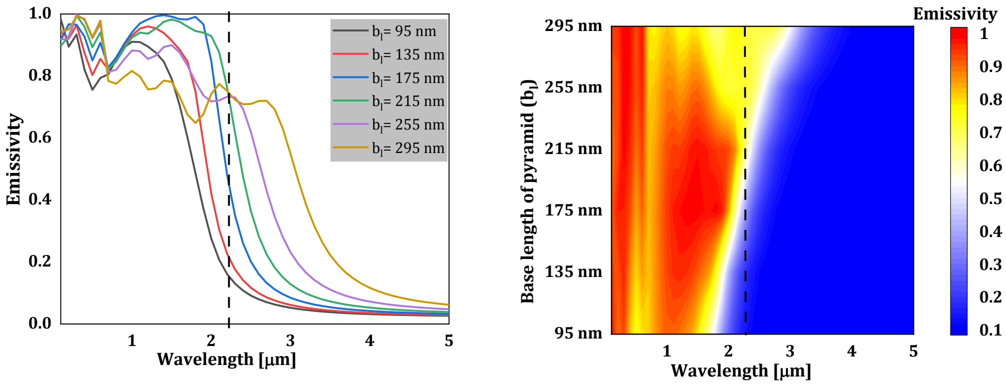

(a) **(b)**

Figure 5: The effect of base length of pyramid (b_1) on the spectral emissivity of proposed nano-pyramid metamaterial with h_1 = 120 nm and h_2 = 115 nm

Figure 6 (a) and (b) illustrate the reflectivity of the designed emitter as b_l optimized from 95 nm to 295 nm. As seen from the figure, when b_l was varied, the reflectivity of the emitter was changed in the opposite direction to the emissivity of the emitter. When b_l was enlarged from 95 nm to 215 nm, the reflectivity before the cutoff wavelength was decreased, whereas if b_l was enlarged from 215 nm to 295 nm, the reflectivity of the emitter was increased by a small value. This result suggested that the emitter's electromagnetic property was influenced by the length of the pyramid

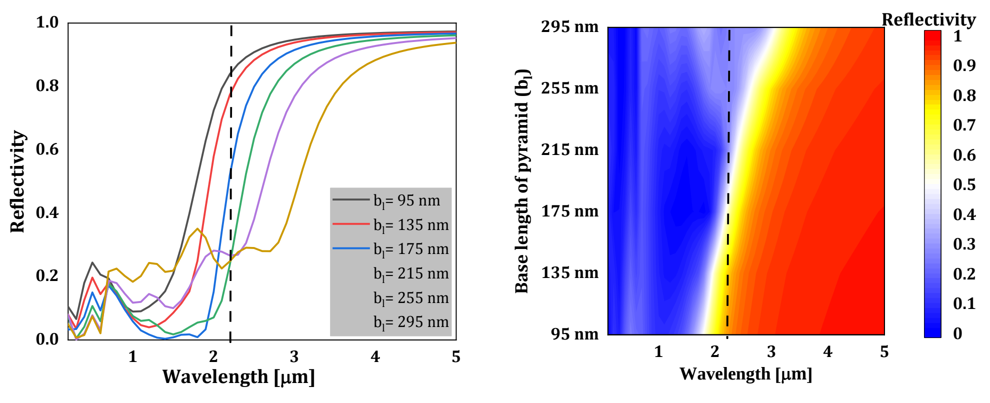

(a) **(b)**

Figure 6: The effect of base length of pyramid (b_1) on the spectral reflectivity of proposed nano-pyramid metamaterial with h_1 = 120 nm and h_2 = 115 nm

To explain the perfect broadband absorption, the electromagnetic field around the nano-pyramid emitter was analyzed. Several excitation mechanisms occurred with resonance frequencies such as MPs, SPP, and high intrinsic loss of tungsten due to design was featured as a Metal-Dielectric-Metal (MDM) structure and the combination of these resonances increased broadband emissivity (Maremi *et al*., 2018). MP is the excitation method that can powerfully localize the electromagnetic energy in the AlN layer, which was inserted between the first W layer and the ground film layer, as well as between two consecutive metal (W) layers (metal-dielectric-metal or W-AlN-W). Due to the existence of free charge on the thin film W surfaces of the ground layer, the first W layer or between two sub-layers in the nano-pyramid, there was a net flow of oscillating electric currents, which resulted in induced magnetic fields. The simultaneous collaboration of magnetic polariton resonances at a targeted wavelength created a near-perfect broadband emissivity

The result of the simulation revealed that the first peak on the graph of figure 6a was excited because of SPP, while the second peak was excited because of MP. As seen on the graph of Figure 6a, the variation of b_l had a significant impact on MP and a little impact on SPP; as a result, b_1 pushes MP to the longer wavelength. The widest and most near-perfect broad band emissivity occurred when b_l = 215 nm (green line), h_1 = 120 nm, and h_2 = 115 nm, which was with consideration of the cut-off wavelength.

4.2. Effect of pyramid height

Figure 7 illustrates the variation of the height of the pyramid on the emissivity of metamaterial with constant base length of the pyramid and dielectric thickness of 215 nm and 115 nm, respectively. As the height of the pyramid enlarged from 40 nm to 240 nm, the emissivity of the designed emitter varied as in figures 7 (a) and (b). As shown in figure 7 (a), the peak occurred in the case of the nano-pyramid; the peak was found at a wavelength of 0.1 µm and the second peak at 2 µm. The result illustrated that as h_1 enlarged from 40 nm to 240 nm, the first peak was increased slightly except for h_1 = 120 nm, whereas the second peak was increased when h_1 varied from 40 nm to 80 nm and when h_1 enlarged from 120 nm to 240 nm, the peak was shifted to the smaller wavelength. It was demonstrated that as the h_1 was optimized from 40 nm to 240 nm, the emissivity of the designed MM was shifted to the shorter wave length and at smaller h_1 (40 nm-80 nm) the emitter had less emissivity before the cutoff wavelength (black dotted line), whereas, at larger h_1 (120 nm-240 nm), the emissivity of the emitter after the cutoff wavelength was decreased

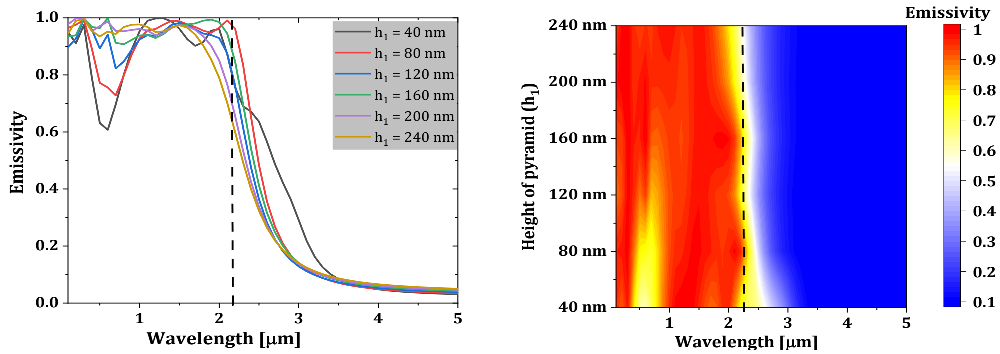

Figure 7: The effect of pyramid height (h_1) on the spectral emissivity of designed nano-pyramid metamaterial with b_1 = 215nm and h_2 = 115 nm

Figure 8 (a) and (b) show the effect of optimizing h_1 from 40 nm to 240 nm on the reflectivity of the designed emitter. As revealed from the graph, the peak reflectivity occurred in the case of the nano-pyramid; the first peak was found at a wavelength of 0.6 µm and the second peak was at 1.7 µm. When h_1 was enlarged from 40 nm to 240 nm, the first peak was decreased rabidly and approached zero, which increased the emissivity of the emitter. The second peak was also decreased and shifted to the longer wavelength. Figure 8 (b) counter fills showed that when h_1 was optimized from 40 nm to 240 nm, the reflectivity of the designed MM shifted to the longer wave length and that at smaller h1 (40 nm–80 nm), the material reflected more than at larger h_1 (120 nm–240 nm) before the cutoff wave length (black dotted line).

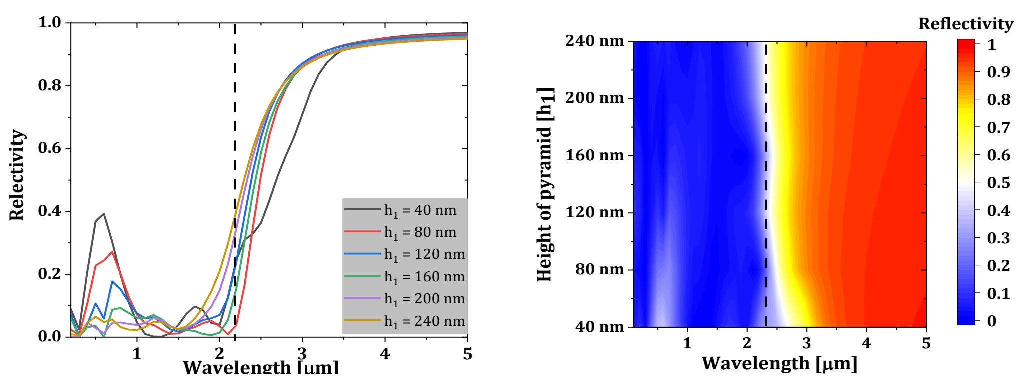

(a) **(b)**

Figure 8: The effect of pyramid height (h_1) on the spectral reflectivity of designed nano-pyramid metamaterial with b_1 = 215nm and h_2 = 115 nm

The simulation results show that when h_1 was optimized from 40 nm to 160 nm before the cutoff wave length (2.2 µm), the average emissivity increased while the average reflectivity decreased, and when h1 was optimized above the cutoff wave length (> 2.2 µm), the average emissivity decreased while the average reflectivity increased. When h1 was enlarged from 160 nm to 240 nm, before cutoff wave length, the average of emissivity decreased slightly and the average of reflectivity increased slightly. The emitter achieved broadband emissivity over 0.1 µm–2.2 µm at h_1 = 160 nm (green line), b_1 = 215 nm, and h_2 = 115 nm.

4.3. Effect of dielectric thickness

The gaps between metalized areas (dielectric thickness) on an MM emitter are crucial in defining the device's resonant frequency. Two metal areas close to one another will induce capacitance, causing the induced fields to change even more. The capacitance, and hence the resonant frequency, will fluctuate when the distance between the metal areas is increased or decreased. A more in-depth examination of these impacts necessitates the use of the Drude model. This model considers electrical conduction in terms of classical collisions; with electrons moving in a straight path until collide with another particle. In terms of classical motion, the rhythmic motion of an electron that is displaced and then drawn back into the plasma to restore neutrality is known as plasma frequency ω_p. The electron overshoots and is dragged back in the opposite direction due to its inertia (Pfiester, 2015). As shown in Equation 25, a material index of refraction, n, may be expressed in terms of plasma frequency ω_p.

$$n^2 = 1 - \frac{{\omega_p}^2}{\omega^2 - j\omega\gamma} \tag{25}$$

where ω is the incident light frequency and is the collision frequency. Similarly, the permittivity, ε, may be stated in plasma frequency terms Equation 26,

$$\varepsilon = 1 - \frac{{\omega_p}^2}{\omega^2 + j\omega\gamma} \tag{26}$$

The plasma frequency will be affected by changes in system capacitance caused by changes in the split gaps or closeness of unit cells. This may be demonstrated using a simple derivation.

Because capacitance is a function of permittivity and the distance between parallel plates, d may approximate the MM pattern as two plates separated by a dielectric as Equation 27,

$$C = \varepsilon \frac{A}{d} \tag{27}$$

A is the area of the plates in this equation, which we may assume will remain constant no matter how far apart they are. By rearranging the equation,

$$\varepsilon = C \frac{d}{A} \tag{28}$$

This may then be entered into Equation 27 and the plasma frequency calculated as Equation 29 is,

$$\omega_p{}^2 = (\omega^2 + j\omega\gamma)\left(1 - \frac{Cd}{A}\right) \tag{29}$$

The plasma frequency of the medium is affected by changes in distance or capacitance, which change the permittivity response. As the gap width widens, the resonance frequency shifts somewhat. Figure 9 shows the effect of dielectric thickness on emitter emissivity at constant pyramid h_1 and b_1.

As the dielectric thickness enlarged from 45 nm to 220 nm, the emissivity of the designed emitter varied as in figures 9 (a) and (b). As shown in figure 9 (a), the peak of emissivity occurred in the case of the nano-pyramid; the first peak was found at a wavelength of 0.1 µm and the second peak was at 2 µm. The result illustrated that as h_2 enlarged from 45 nm to 220 nm, the first peak was increased and shifted to the longer wavelength, whereas the second peak was increased when h_2 varied from 45 nm to 80 nm and shifted to the smaller wave length. Also, when h_1 enlarged from 80 nm to 220 nm, the peak was decreased rapidly and shifted to a shorter wave length. It was demonstrated that as the h_2 was optimized from 45 nm to 80 nm, the emissivity of the designed MM was increased below the cutoff wavelength (black dotted line) and decreased after the cutoff wavelength, whereas, as h_2 was optimized from 80 nm to 220 nm, the emissivity below the cutoff wavelength was decreased.

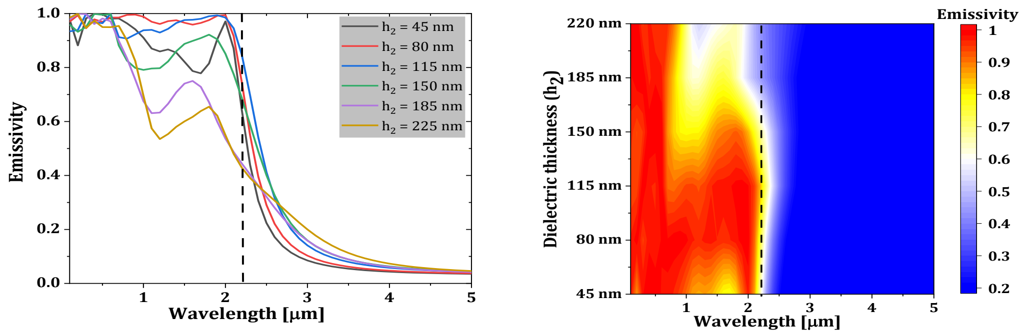

(a) **(b)**

Figure 9: The effect of dielectric thickness (h_2) on the spectral emissivity of designed nano-pyramid metamaterial with b_1 = 215 nm and h_1 =160 nm

Figure 10 (a) and (b) show the effect of optimizing h_2 from 40 nm to 220 nm on the reflectivity of the designed emitter. As revealed from the graph, the peak occurred in the case of the nano-pyramid; the peak was found at a wavelength of 0.2 μm and the second peak at 1.6 μm. When h_1 was enlarged from 45 nm to 220 nm, the first peak was decreased rabidly and approached zero, which increased the emissivity of the emitter. The second peak was also decreased when h_2 varied from 45 nm to 80 nm, but when h_2 enlarged from 80 nm to 220 nm, the peak was increased and shifted to the shorter wavelength. The counter fills also illustrated that when h2 was optimized from 45 nm to 80 nm, the reflectivity of the designed MM was shifted to the longer wave length and when h_2 was enlarged from 80 nm to 220 nm, the reflectivity of the designed MM was shifted to the shorter wave length. At smaller h_2 (45 nm – 80 nm), the material was reflected less before the cutoff wavelength (black dotted line) and at larger h_2 (80 nm-220 nm), the material reflected more than at smaller h_2 (45 nm – 80 nm).

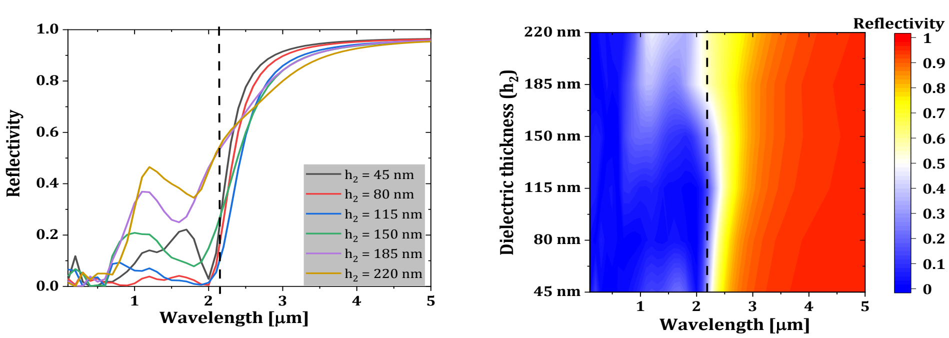

(a) **(b)**

Figure 10: The effect of dielectric thickness (h_2) on the spectral reflectivity of designed nano-pyramid metamaterial with b_1 = 215 nm and h_1 =160 nm

According to the simulation results, when h2 was optimized from 45 nm to 80 nm before the cutoff wave length (2.2 µm), the average emissivity increased and the average reflectivity decreased, whereas when h2 was optimized above the cutoff wave length (> 2.2 µm), the average emissivity decreased and the average reflectivity increased. When h_2 enlarged from 80 nm to 220 nm, before cutoff wave length, the average of emissivity decreased and the average of reflectivity increased. The emitter achieved broadband emissivity over 0.1 m–2.2 m at h_2 = 80 nm (red line), b_1 = 215 nm, and h_1 = 160 nm.

4.4. Angular Emissivity

The character of the angular emissivity of the TPV emitter is important due to the polarization angles of electromagnetic waves. Figure 11 (a) and (b) explain the effect of polarizations and incident angles on the spectral emissivity of the designed selective metamaterial emitter with optimized geometric parameters h_1 = 160 nm, h_2 = 80 nm, and b_1 = 215 nm. Nonetheless, the result of Figure 11 (a) suggests that the designed metamaterial emitter is independent of polarization angle by making incident angle 0°. This explains that the designed emitter had symmetry. The result of figure 11 (b) demonstrated that as the incident angle increased from 0° to 60°, the emittance curve did not change considerably. When the incident angle was set to 75°, the emissivity decreased slightly; however, it maintained a good emittance. This result shows that the emitter is suitable for plane waves with a wide range of incident angles from 0° to 60°.

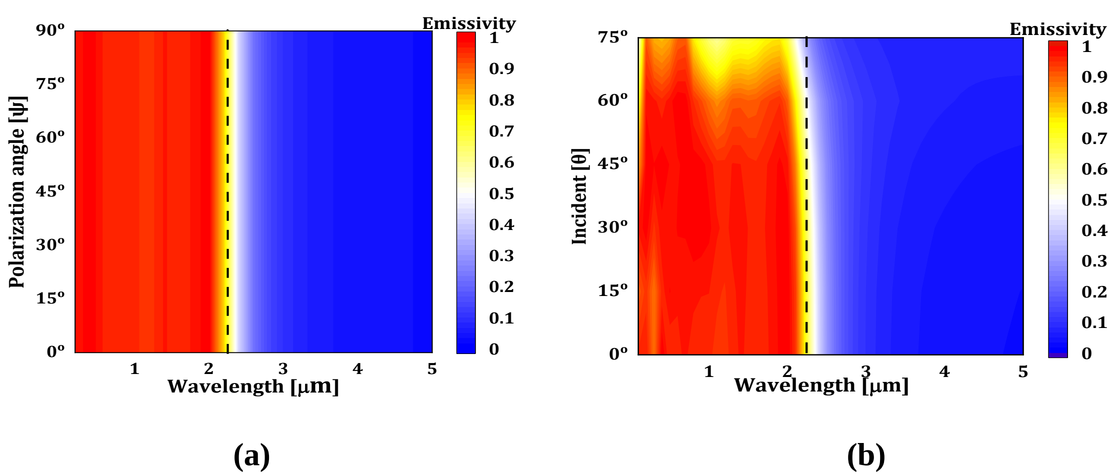

Figure 11: (a) The effect of polarization angle (ψ) on the spectral emissivity of designed nano-pyramid MM emitter (b) The effect of incident angle (θ) on the spectral emissivity of designed nano-pyramid MM emitter

4.5. Distribution energy flow

At specific wavelengths, an electromagnetic wave moving in space contains energy and is absorbed by the MTM. To enlighten at specific wavelengths, an electromagnetic wave moving in space contains energy and is absorbed by the MTM (Maremi *et al*., 2018). The distributions of the Poynting vector in the MTM emitter are displayed in Figure 12 to illustrate the process of strong emission. The energy flow density vector in an electromagnetic field is represented by the Poynting vector,

$$S = \frac{Re(E \times H^*)}{2} \qquad (30)$$

where, S is the Poynting vector, Re is real, E is the electric field, and H^* is the complex conjugate of magnetic field. As shown in Figure 12, the proposed emitter had a substantial energy flow at wavelengths of 1.6 µm and 2 µm with emissivity amplitudes of 0.958 and 0.994, respectively, and the energy distribution was also greater at 2 µm due to the emissivity amplitude. However, with a wavelength of 5 µm and emissivity amplitude of 0.03, there was minimal energy flow in the emitter. As a result, high energy distributions were associated with high emittance, while low energy distributions were associated with low emittance.

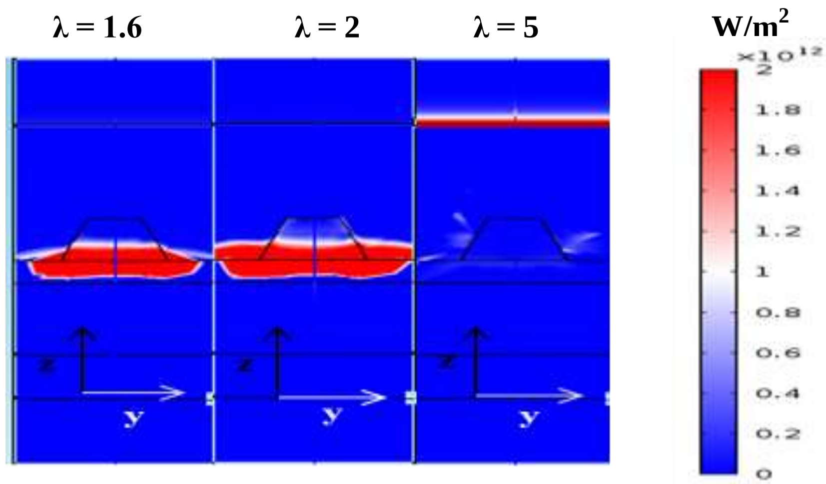

Figure 12: The distribution of energy flow (Poynting vector) at wavelengths 1.6 µm, 2 µm, and 5 µm of within a nano-pyramid emitter

4.6. Performance of TPV

Figure.13 (a) presents the emission, reflection, and transmission spectra of the optimized emitter at b_1 = 215 nm, h_1 = 160 nm, h2 = 80 nm, h_3 = 260 nm, and w = 395 nm. As seen from figure 14 (a), the transmission of the designed emitter was zero. This was because AlN prevented transmission and ground W reflection. Due to the high intrinsic loss of tungsten and coupling MP and SPP resonance modes, the designed emitter was reflected near zero before cutoff wavelength (2.2 µm) and above cutoff wavelength (> 2.2 µm). The constructed emitter achieved high emissivity before 2.2 µm (shaded area) of about 96.4% and low emissivity above 2.2 µm. This was attained by optimizing the geometric parameters such as b_1, h_1 and h_2. Figure 14 (b) illustrated the emissivity above 4 nm at b_1 = 215 nm, h_1 = 160 nm, h2 = 80 nm, h_3 = 260 nm, and w = 395 nm. As seen from the graph, the emissivity of the designed MM was decreased dramatically as wavelength increased and the emissivity was less than 5% above 4 µm. This enabled the emitter to enhance spectral efficiency.

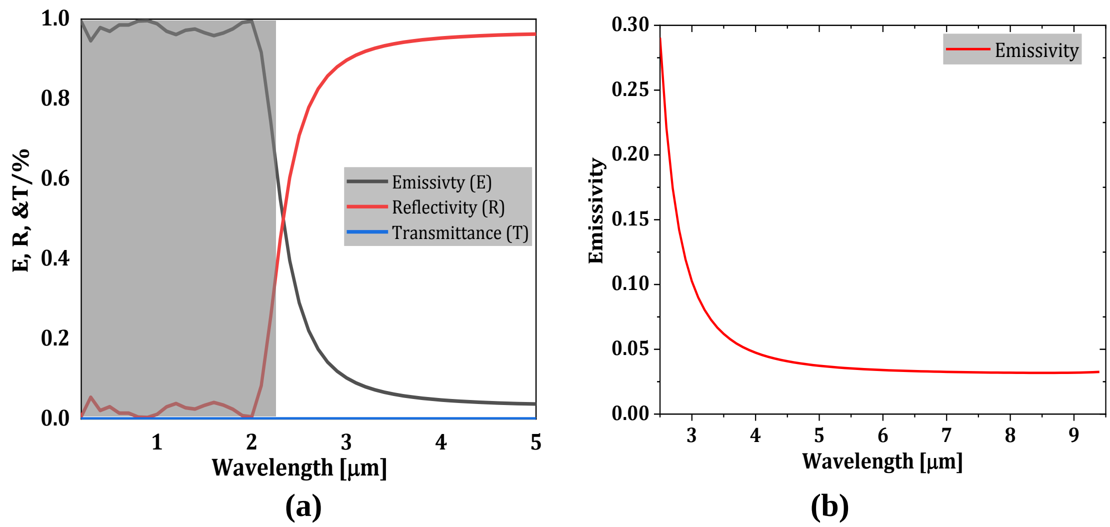

Figure 13: (a) Emissivity, Reflectivity, and Transmittance of the designed nano- pyramid emitter with cutoff wave length 2.2 µm (b) The emissivity of nano-pyramid emitter above 2.5 µm

Figure 14 (a) shows the spectral emissivity of designed TPV emitter with and without nano-pyramid at b_1 = 215 nm, h_1 =160 nm, h_2= 80 nm, h_3 = 260 nm, and w = 395 nm. As seen from the figure six peak on the designed emitter with nano pyramid, the first peak was obtained at short wave length λ = 0.2 µm with an amplitude of 0.99398 which was obtained because of excitation of SPP between AlN and bottom W. Also, there was another peak at long-wavelength λ = 2 µm with an amplitude of 0.99454 that revealed because the MP through the coupling between magnetic resonance inside the nano-pyramid and the incident electromagnetic wave through in port. When the emitter was designed without nano-pyramid or only from bottom W and AlN, the emissivity in the shaded area was decreased and the peak obtained at λ= 0.1 µm and 0.7 µm with amplitude 0.9733 and 0.957 respectively because of SPP. However, when nano-pyramid was added or when the design contained W-AlN-W, the emissivity in the shaded area was increased and the first peak was increased and shifted to the longer wave length, as well as the second peak was increased. Also, due to the excitation of MP through the coupling between diamagnetic response inside the nano-pyramid and bottom tungsten, high emissivity was achieved by using the suggested design.

Figure 14 (b) demonstrated that the emissivity of designed nano-pyramid metamaterials with those of existing thermal emitter metamaterials, with the shaded area indicating the EQE of InGaAs. Here, InGaAs was used as TPV cell in this work due to its higher EQE before 2.2 µm than the other cell as shown figure 14 (c), which has 0.55 eV band gap energy (Shoaei, 2016). The blue line shows the designed selective emitter emissivity, whereas the black line represents Wolf *et al*., (2014) and the red line represents Merami *et al*., (2018). As observed from figure 14 (b), the emitter was nearly perfect broadband above the band gap of InGaAs (shaded area or > 2.2 µm), and dramatically dropped below the band gap of InGaAs (out of shaded area or < 2.2 µm). Because of the presence of a band gap in the TPV cell, radiation energy below the band gap was deemed waste energy, whereas radiation energy above the band gap was required (convertible) energy. As a result, this finding was showed that the designed emitter was produced highly convertible photons.

The red and black lines in the figure 14 (b), depicting spectral emissivity were created using an InGaAs TPV cell with a cut-off wavelength of 2.1 µm. The black line exhibits virtually perfect broadband emissivity at wavelengths less than 1.4 µm, beyond which it drops rapidly, and the red line shows broadband emissivity up to 2.1 µm cutoff wavelengths. For high spectral efficiency of the TPV emitter, this work improved virtually perfect broadband emissivity from 0.1 µm to 2.2 µm cut off wavelength which was the widest from Wolf *et al*., (2014) and Merami *et al*., (2018). The average spectral emissivity with a band gap of 0.2 µm to 2.1 µm was around 96.6% and 79.7% for the red and black lines, respectively, and for the blue line the average emissivity in a wavelength range of 0.1 µm to 2.1 µm 97.4%. This demonstrated that the developed nano-pyramid emitter had superior average spectral emissivity than Wolf *et al*., (2014) and Merami *et al*., (2018).

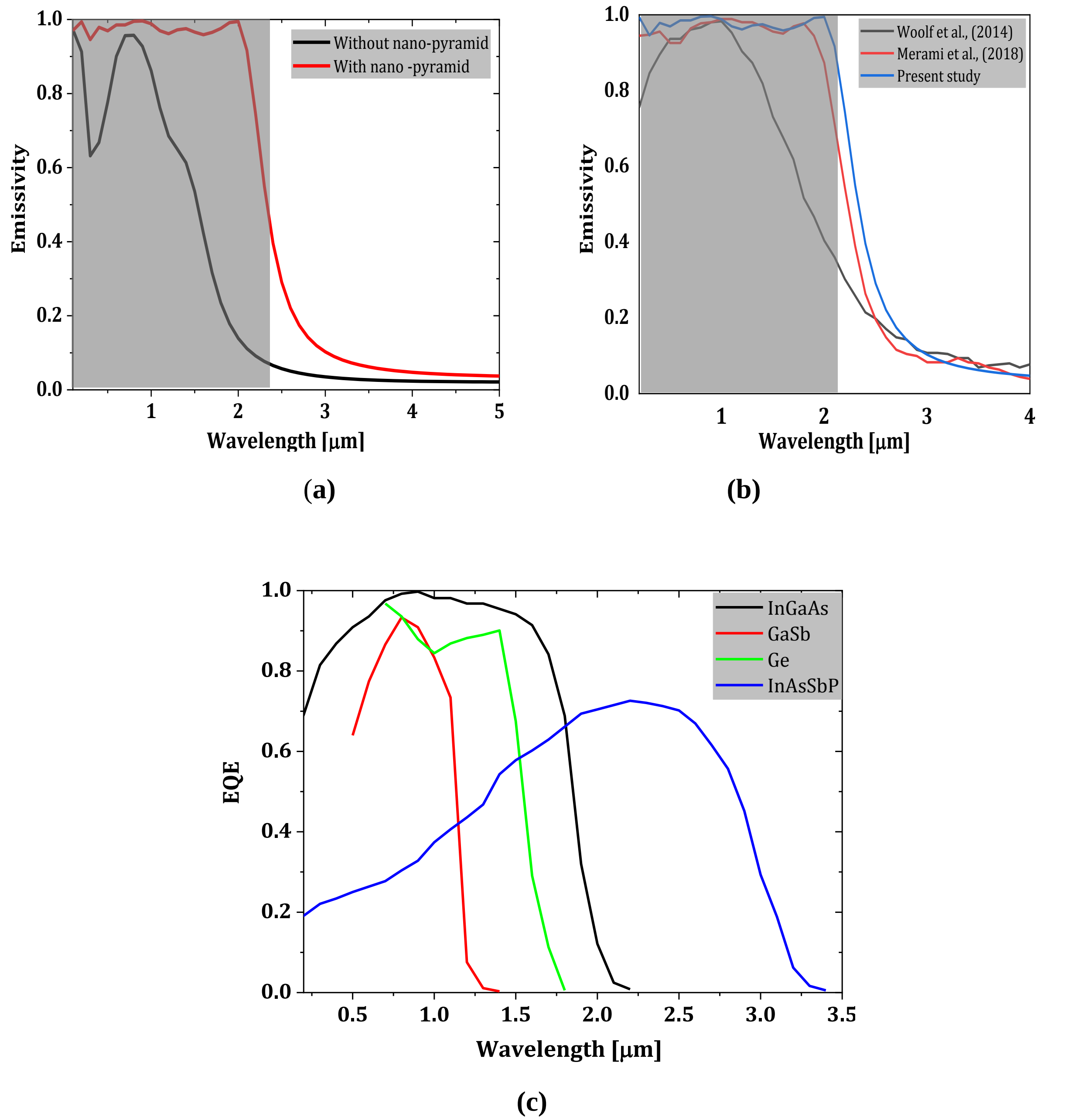

Figure 14: (a) The spectral emissivity of designed TPV emitter with and without nano-pyramid (b) The spectral emissivity of suggested emitter with Woolf *et al*., (2014) and Merami *et al.*, (2018) for EQE of InGaAs and (c) The EQE of different TPV cell (Shoaei, 2016)

The TPV cell converts the emissivity above its band gap energy or below cutoff wave length, so high emissivity before cutoff wavelength and low emissivity above cutoff wavelength are the factors that required when designing an emitter, particularly to enhance the performance of TPV system. This work developed a nano-pyramid metamaterial that improves spectral efficiency in a TPV system. To evaluate the efficiency of an optimized emitter for a TPV cell, the efficiency of the TPV system was analyzed. The efficiency of a TPV system to convert radiated heat to electrical power is given by Equation (31) (Gu *et al*., 2015) gives the efficiency of a TPV system in converting radiated heat to electrical power,

$$\eta_{TPV} = \eta_{SP}\eta_{PV} = \frac{P_{out}}{P_{rad}} \tag{31}$$

where, $\eta_{SP}$the spectral efficiency of the emitter, η_{PV} is the efficiency of the photovoltaic cell, P_{out} is the maximum output power, and P_{rad} is the total radiant power from an emitter. Spectral efficiency η_{SP} is defined by equation,

$$\eta_{SP} = \frac{\int_0^{\lambda_c} E(\lambda)\varepsilon(\lambda)d\lambda}{\int_0^{\infty} E(\lambda)\varepsilon(\lambda)d\lambda}, \tag{32}$$

where, λ_c is the cut-off wavelength, $E(\lambda)$is emission spectrum of a blackbody which calculated as equation 9, and $\varepsilon(\lambda)$ is spectral emissivity of the proposed selective emitter metamaterial (Maremi *et al*., 2018).

The spectrum irradiance of both the optimized nano- pyramid selective emitter and the black body at different temperatures was examined. Equation (32) can be used to compute spectral efficiency, and Equation (9) can be used to calculate $E(\lambda)$. When the selective emitter has excellent emissivity below the cut-off wavelength and poor emissivity above the cut-off wavelength, the highest efficiency was reached. Figure 15 (a) and (b) compare the spectrum irradiance of the black body with selective designed emitter, at temperatures ranging from 900 K to 1600 K. The spectral irradiance improved as the temperature enhanced, indicating that the emission peak was changed to a lower wavelength as the temperature increased, as explained by Wien's law, and this indicated that the emission spectrum peak was above the band gap area. The optimized nano - pyramid MM emitter was resulted high emissivity at h_3 = 260 nm, w = 395, h_1 = 160 nm, h_2 =80 nm, and b_l = 215 nm, before cutoff wavelength.

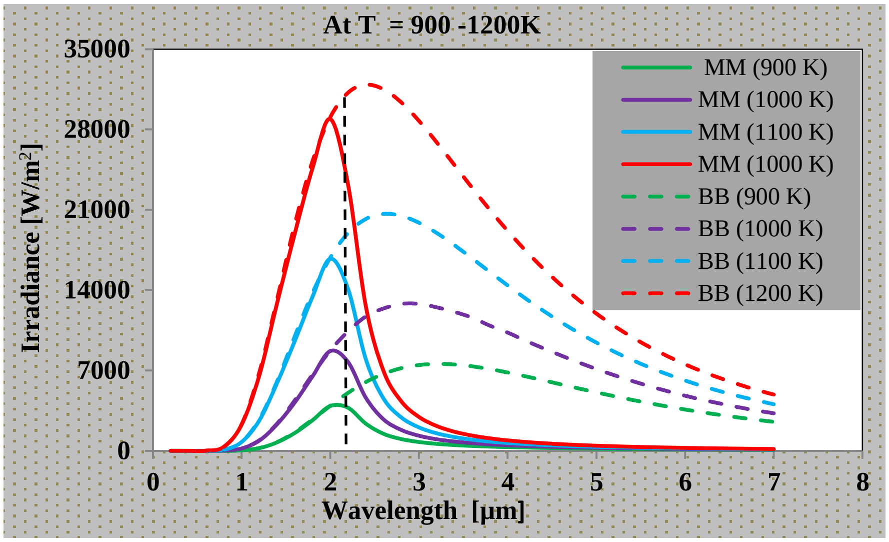

(a)

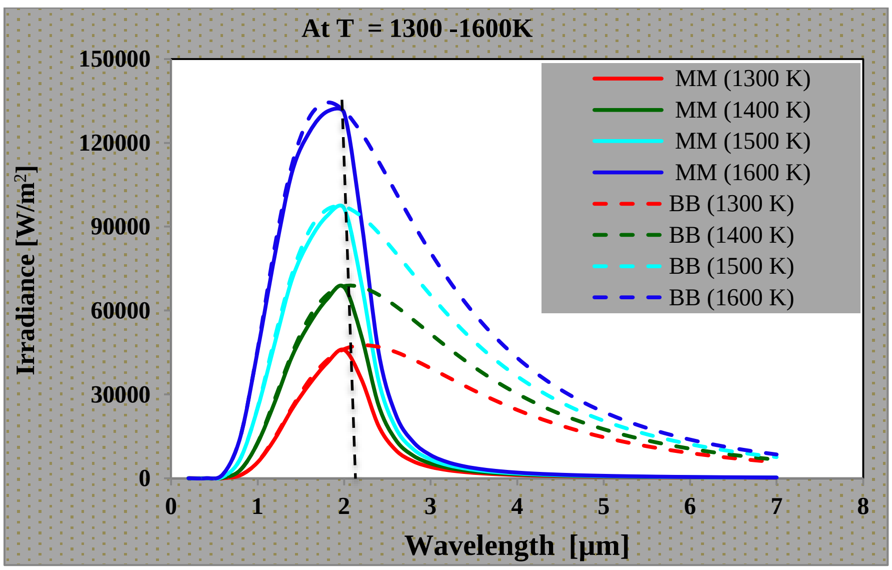

(b)

Figure 15: Illustrate the comparison of the suggested emitter with the blackbody in terms of spectral emissivity at different temperature

The solid line on the graph of figures 15 (a) and (b) was the emissivity of the designed nano-pyramid emitter, while the dotted line was the emissivity of the blackbody. When comparing the suggested emitter to the blackbody in terms of spectral emissivity at different temperatures, as shown in figures 15(a) and (b), the designed nano-pyramid emitter exhibited selective emission above the band gap. The vertical black dot line on both graphs indicates the cutoff wavelength of InGaAs, which is about 2.2 µm. The spectral irradiance of the black body above the cutoff wavelength (dotted line) was higher than the spectral irradiance of the designed nano-pyramid emitter. This shows that the emitter decreased the waste spectral irradiance that heated the TPV cell. Due to this, the emitter was able to achieve high performance by increasing the efficiency of the TPV system.

The spectral efficiency of the emitter at different temperatures, which was calculated according to Equation (32) above, can be given in table 1. When compared to Woolf et al. (2014), who achieved spectral efficiency of 43% and 52%, and Merami et al. (2018), who achieved spectral efficiency of 76% and 82.4% at 1300 K and 1500 K, respectively, the results show the spectral efficiency of the designed emitter was 78.6% and 84% at 1300 K and 1500 K, respectively for the EQE of InGaAs, which was the highest. As demonstrated in Equation (31), excellent spectral efficiency was required to enhance the efficiency of TPV systems, and this study optimized the spectral efficiency more than the previous study. The result of spectral efficiency was expressed as that as the temperature was raised, the spectral efficiency of both the MM emitter and black body was increased. That shifted the peak of spectral irradiance to the left (a shorter wavelength).

Table 1: Spectral efficiency of designed emitter calculated at different temperature

Temperature	**MM Spectral efficiency**
900K	56%
1000K	64%
1100K	70.2%
1200K	75%
1300K	78.6%
1400K	81.7%
1500K	84%
1600K	86.3%

Figure (16) illustrates the comparison of the spectral efficiency of a designed emitter with the black body. The black histogram represented the spectral efficiency of blackbody, whereas the light blue histogram represented the spectral efficiency of designed nano-pyramid. As seen from the figure, the spectral efficiency of the nano-pyramid MM emitter was higher than the blackbody. This shows the designed emitter was able to convert more radiated energy than the black body. For example, the black body converted 25% of radiated energy at 1200 K; however, the designed nano-pyramid metamaterial converted 75% of radiated energy at a similar temperature to the black body, demonstrating that at 1200 K, the suggested emitter increased the efficiency of the TPV system three times. Furthermore, the figure explains that as the temperature was raised, the spectral efficiency of both the blackbody and the supposed emitter was dramatically increased. Additionally, the designed emitter was more efficient and converted higher radiated energy at lower temperatures than the black body. For example, the black body converted only 6% and 12% of radiated energy at 900 K and 1000 K respectively, but the suggested nano-pyramid TPV emitter converted 56% and 64% at 900 K and 1000 K respectively. This shows that the designed emitter increased the efficiency of the TPV system by 9.3 and 5.3 times, respectively.

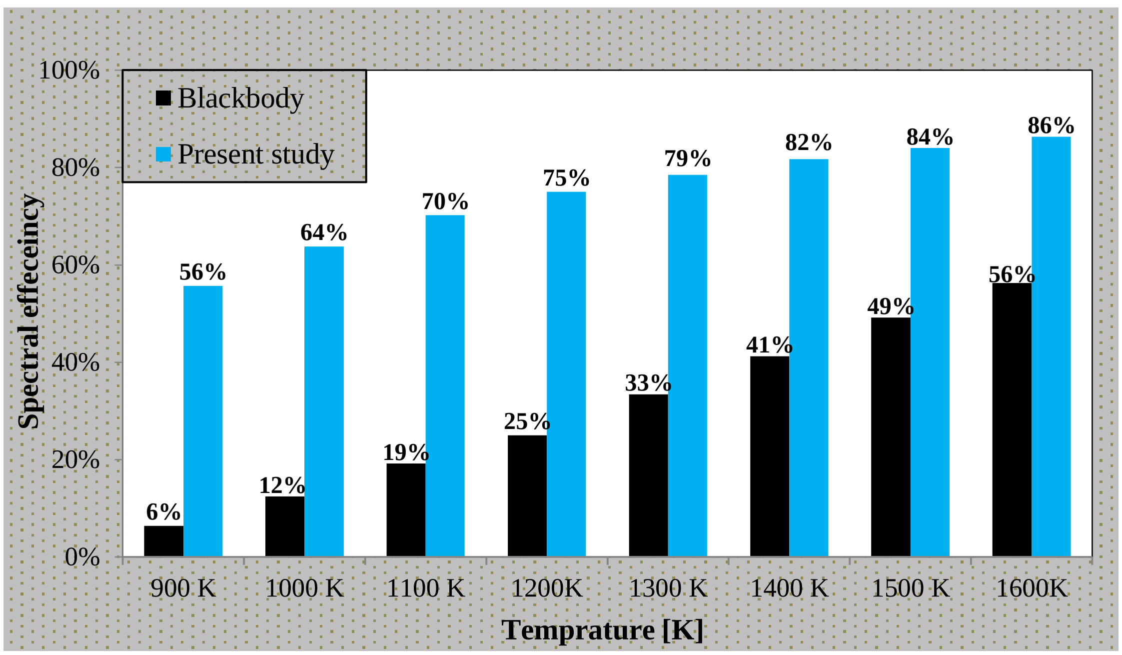

Figure 16: Comparison of designed nano-pyramid emitter spectral efficiency with blackbody spectral efficiency

Figure 17 shows a comparison of the proposed nano-pyramid metamaterial spectral efficiency with the spectral efficiency of blackbody and Jiang *et al*. (2019) at 800K, 1000K, and 1200K. The green histogram shows the designed selective emitters' spectral efficiency; whereas the black histogram represents the black body and the blue histogram represents Jiang *et al*. (2019). The black and blue histograms in the picture depict the spectral efficiency of the blackbody and a multilayer MM emitter for EQE of InGaAsSb at 800 K, 1000 K, and 1200 K, respectively, whereas the light blue histogram shows the spectral efficiency of the designed metamaterial for EQE of InGaAsSb. As shown in the figure, the blackbody convert 3%, 13%, and 29% of radiated energies at 800 K, 1000 K, and 1200 K respectively, and the multilayer-ring of Jiang *et al*. (2019) converts 36.4%, 58%, and 72% of radiated energy at similar temperatures for the EQE of InGaAsSb. However, the designed emitter converts about 58%, 74%, and 83% of the radiated energy at 800 K, 1000 K, and 1200 K, respectively, for the EQE of InGaAsSb. This result shows that high radiated energy was more convertible by designed nano-pyramid emitters than blackbody and Jiang *et al*. (2019).

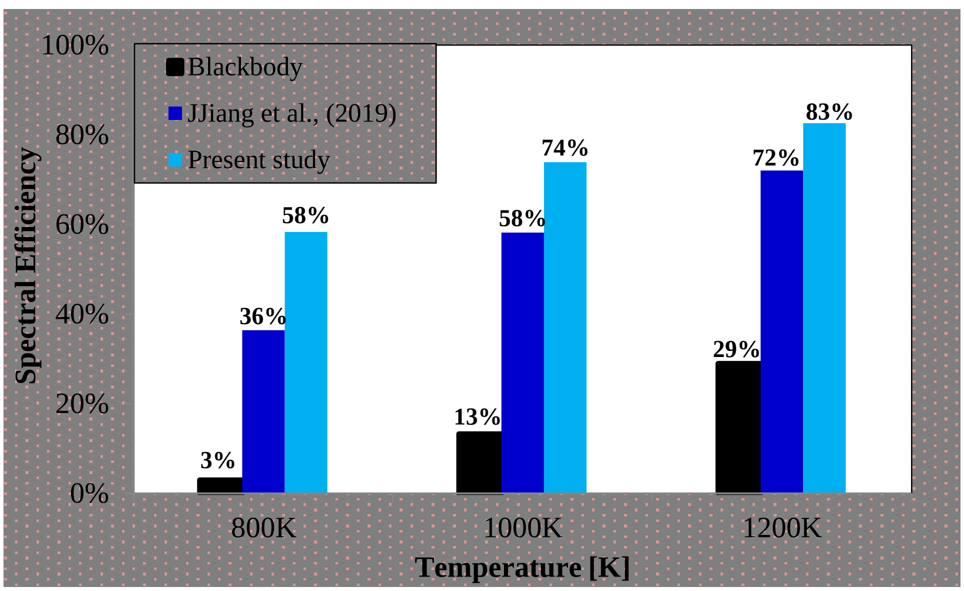

Figure 17: Comparison of the proposed nano-pyramid metamaterials spectral efficiency with the spectral efficiency of blackbody and Jiang *et al*., (2019) at 800K, 1000K and 1200 K for EQE of InGaAsSb

Table 2 compares the materials used and the emissivity generated by other metamaterial emitters with the designed nano-pyramid emitter. The suggested emitter was achieved across a wide range of wavelengths from 0.1 µm to 2.2 µm with a high emissivity of about 0.964, which was higher than those given in below table 2. Further, Different scholars have designed metamaterial emitters with different materials and geometry. For instance, Wang *et al*., (2015) designed an emitter from W at the bottom metal, Magnesium Fluoride (MF_2) as a dielectric spacer, and Titanium (Ti) at the top by the design of a pyramid nanostructure, Song *et al*., (2016) designed 2D trilayer films, Merami *et al.*, (2018) created a multilayer ring geometry grating from W and AlN, Jiang *et al*., (2019) created a multilayer ring geometry grating from W and SiO_2, and Abdel-Latif *et al*., (2021) created a 2D cylindrical gear grating from W and SiO_2. Their emissivity and the range of wavelength they absorb are given in the tabular form below.

Table 2: Comparisons between the designed emitter and other emitters at room temperature

	Materials		Emissivty	Range of wavelength
	Metal	Dielectric		
Wang *et a*l., (2015)	W,Ti	MF_2	0.925	500 - 2200 nm
Song *et al*., (2016)	W	SiO_2	0.801	200 - 2200 nm
Merami *et al*., (2018)	W	AlN	0.938	200 - 2200 nm
Jiang *et al*., (2019)	W	Al_2O_3	0.943	500 - 2200 nm
Abdel-Latif *et al*., (2021)	W	SiO_2	0.853	300 - 2200 nm
Present study	W	AlN	0.964	100 - 2200 nm

Figure 18 shows the comparison of designed emitter emissivity with other emitters for EQE of InGaAs (shaded area). As seen from the figure, the emissivity of the designed metamaterial emitter (yellow line) was the highest emissivity in the shaded area and low emissivity above the cut off wave length (out of the shaded region). This shows that the nano-pyramid MM emitter was superior to other emitters.

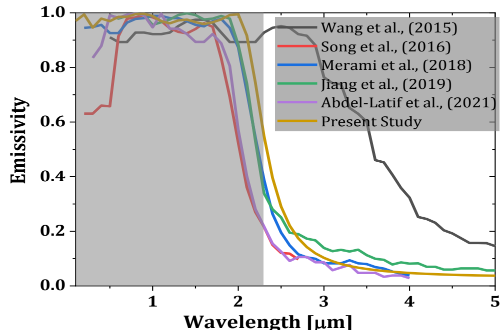

Figure 18: The comparison of designed MM emitter with other emitter for EQE of InGaAs

4.7. Performance of the suggested TPV emitter with Different materials

The performance of the suggested TPV emitter with different materials was as follows in this investigation (Figure 19). The impact of metals such as AlN, Mo, and W on the dielectric substance AlN is seen in Figure 19 (a). The emissivity spectra of Al show poor emissivity across a wide wavelength range of 0.1 µm to 2.2 µm. In the visible and near-IR wavelengths, aluminum metal suffers considerable losses. The optical characteristics of the Al could not be modified because of its significant negative real permittivity value. The Mo, on the other hand, showed a low emissivity in the shaded area (before cutoff wavelength). Within the wavelength range under consideration, the emissivity of the designed TPV emitter with AlN/W is clearly better. Figure 19 (b) depicts the influence of the proposed nano-pyramid TPV emitter on several dielectric materials such as Al_2O_3, SiO_2, and AlN. The spectrum emissivity of AlN dielectric material was high emissivity at specific wavelengths from 0.1 µm to 2.2 µm and decrease at long wavelength as indicated in the graph.

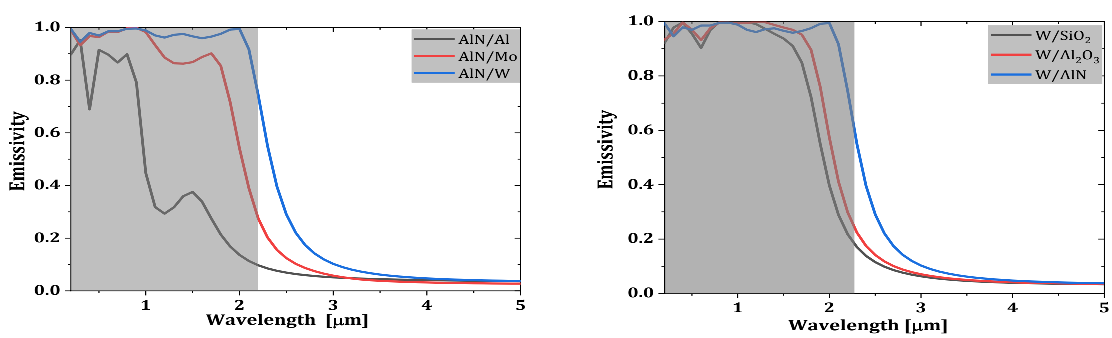

(a) **(b)**

Figure 19: The emittance spectra of the nano-pyramid TPV emitter using (a) AlN with different metal (b) W with different dielectric material of the suggested TPV emitter

5. Conclusion and Recommendation

5.1 Conclusion

A wavelength-selective TPV metamaterial emitter based on a nano-pyramid from tungsten and aluminum nitride spacer which has a cutoff wavelength match to InGaAs with band gap energy of 0.55 eV was numerically designed and analyzed. The spectrum emissivity of the suggested TPV emitter was strongly affected by the geometrical parameters through the wavelength range from 0.1 µm to 2.2 µm. Therefore, the impact of the base length of the pyramid (b_l), the height of the pyramid (h_1), and dielectric thickness (h_2) were studied to optimize the calculated emissivity. The proposed metamaterial increased the efficiency of the TPV system. Efficiency was also enhanced when all radiated photons were absorbed by the TPV cell. At w = 395 nm, h_3 = 260 nm, h_1 = 160 nm, h_2 = 80 nm, and b_1 = 215 nm, the designed metamaterial emitter exhibited an enhanced near-perfect broadband and wide-angle average of emissivity of about 96.4% between the wavelengths of 0.1 µm and 2.2 µm, whereas the emissivity above 2.2 µm was dramatically decreased. This resulted in the enhancement of the spectral efficiency of the emitter. The designed metamaterial emitter showed polarization independence and achieved high emissivity over a wide range of incident angles from 0 to 60^0. This MM emitter also achieved high spectral efficiency when constructed from W and AlN rather than the other materials. In this work, the comparison of designed emitter spectral efficiency with blackbody spectral efficiency for EQE of InGaAs was also studied. The result explained that the designed emitter achieved higher spectral efficiency than the black body. Furthermore, the designed emitter increased the efficiency of the TPV system by 9.3, 5.3, 3.68, and 3 times blackbody at 900K, 1000 K, 1100 K, and 1200 K, respectively. Moreover, at 800 K, 1000 K, and 1200 K, the spectral efficiency of the designed emitter was compared to that of the black body and Jiang *et al.*, (2019) for EQE of InGaAsSb. The results showed that the nano-pyramid emitter had the highest spectral efficiency than both. In general, for the TPV system of the InGaAs cell, the designed metamaterial emitter demonstrated spectral efficiency of about 75% and 86.2% at 1200K and 1600K, respectively, which was highest when compared to the blackbody and previous scholar MM emitter. This shows that the designed emitter has great significance in order to enhance the efficiency and performance of the TPV system.

5.2 Recommendation

The rapid depletion of fossil resources, along with the growing need for energy, has prompted a global call to improve energy conversion efficiency. Typical fossil fuel power production plants have a low energy conversion rate, and large portion of the energy is lost as heat which contributing to the global warming problems. Reusing and recovering even a small portion of energy sufferers could provide a huge impact on energy saving and reduce the dependence on fossil fuels. The TPV system appears to be a viable option for capturing, recovering and converting waste heat energy into usable electricity. Each component in the TPV system thermal emitter and TPV cells is vital and can be engineered to achieve a better heat-to-electricity conversion efficiency. To achieve great efficiency all of these components should be carefully developed and I recommend that the TPV emitter be studied further for maximizing the conversion efficiency and performane TPV system.

Research Found Acknowledgment

This research project is funded by Adama Science and Technology University under the grant number ASTU/SM-R/398/22, Adama, Ethiopia.

Reference

Abdel-Latif, G. Y., Hameed, M. F. O., & Obayya, S. S. A. (2021). Characteristics of thermophotovoltaic emitter based on 2D cylindrical gear grating. *Optical and Quantum Electronics*, *53*(3), 1-14..

Babiker, S. G., Sid-Ahmed, M. O., Yong, S., Ming, X., Choi, Y., Lim, Y., ... & Babu, K. J. (2014). Performance of One-Dimensional Multilayer Nanostructure Emitter and Filter for Thermophotovoltaic applications. *Int. J. Energy, Inf. Commun*, *5*(4), 1-16.

Basu, S., Chen, Y. B., & Zhang, Z. M. (2007). Microscale radiation in thermophotovoltaic devices—a review. *International Journal of Energy Research*, *31*(6-7), 689-716.

Bauer, T. (2011). *Thermophotovoltaics: basic principles and critical aspects of system design*. Springer Science & Business Media.

Bermel, P., Ghebrebrhan, M., Harradon, M., Yeng, Y. X., Celanovic, I., Joannopoulos, J. D., & Soljacic, M. (2011). Tailoring photonic metamaterial resonances for thermal radiation. *Nanoscale research letters*, *6*(1), 1-5.

Bitnar, B. (2003). Silicon, germanium and silicon/germanium photocells for thermophotovoltaics applications. *Semiconductor science and technology*, *18*(5), S221.

Bitnar, B., Durisch, W., & Holzner, R. (2013). Thermophotovoltaics on the move to applications. *Applied Energy*, *105*, 430-438.

Branson, J. (2013). Quantum Physics. *University of California San Diego, Lecture*.

Chan-Olmsted, S. M. (2019). A review of artificial intelligence adoptions in the media industry. *International Journal on Media Management*, *21*(3-4), 193-215.

Chen, Y. B., & Zhang, Z. M. (2007). Design of tungsten complex gratings for thermophotovoltaic radiators. *Optics communications*, *269*(2), 411-417.

Chubb, D. (2007). *Fundamentals of thermophotovoltaic energy conversion*. Elsevier.

Datas, A., & Martí, A. (2017). Thermophotovoltaic energy in space applications: Review and future potential. *Solar Energy Materials and Solar Cells*, *161*, 285-296.

Datas, A., Ramos, A., Martí, A., del Cañizo, C., & Luque, A. (2016). Ultra high temperature latent heat energy storage and thermophotovoltaic energy conversion. *Energy*, *107*, 542-549.

Deng, H., Wang, T., Gao, J., & Yang, X. (2014). Metamaterial thermal emitters based on nanowire cavities for high-efficiency thermophotovoltaics. *Journal of Optics*, *16*(3), 035102.

Ellabban, O., Abu-Rub, H., & Blaabjerg, F. (2014). Renewable energy resources: Current status, future prospects and their enabling technology. *Renewable and sustainable energy reviews*, *39*, 748-764..

Ferroukhi, R., Renner, M., García-Baños, C., Elsayed, S., & Khalid, A. (2020). Renewable Energy and Jobs: Annual Review 2020.

Fleming, J. G. (2005). Addendum:“Three-Dimensional Photonic-Crystal Emitter For Thermal Photovoltaic Power Generation”[Appl. Phys. Lett. 83, 380 (2003)]. *Applied Physics Letters*, *86*(24), 380..

Fowles, G. R. (1989). *Introduction to modern optics*. Courier Corporation.

Fraas, L. M. (2014). *Low-cost solar electric power* (p. 97). New York: Springer.

Fraas, L. M., Avery, J. E., Daniels, W. E., Huang, H. X., Malfa, E., Venturino, M., ... & Wuenning, J. G. (2003, January). TPV tube generators for apartment building and industrial furnace applications. In *AIP Conference Proceedings* (Vol. 653, No. 1, pp. 38-48). American Institute of Physics..

Gamel, M., Jern, K. P., Rashid, E., Jing, L. H., Yao, L. K., & Wong, B. (2019, July). Effect of front-surface-field and back-surface-field on the performance of GaAs based-photovoltaic cell. In *2019 IEEE International Conference on Sensors and Nanotechnology* (pp. 1-4). IEEE..

Gamel, M. M. A., Lee, H. J., Rashid, W. E. S. W. A., Ker, P. J., Yau, L. K., Hannan, M. A., & Jamaludin, M. (2021). A Review on Thermophotovoltaic Cell and Its Applications in Energy Conversion: Issues and Recommendations. *Materials*, *14*(17), 4944..

Gu, W., Tang, G., & Tao, W. (2015). High efficiency thermophotovoltaic emitter by metamaterial-based nano-pyramid array. *Optics express*, *23*(24), 30681-30694..

G Gu, W., Tang, G., & Tao, W. (2015). High efficiency thermophotovoltaic emitter by metamaterial-based nano-pyramid array. *Optics express*, *23*(24), 30681-30694.

Hirst, L. C., & Ekins-Daukes, N. J. (2011). Fundamental losses in solar cells. *Progress in Photovoltaics: Research and Applications*, *19*(3), 286-293.

Hitchcock, C., Gutmann, R., Borrego, J., Ehsani, H., Bhat, I., Freeman, M., & Charache, G. (1997, March). GaInSb and GaInAsSb thermophotovoltaic device fabrication and characterization. In *AIP Conference Proceedings* (Vol. 401, No. 1, pp. 89-103). American Institute of Physics..

Jeffery, D. J. (2001). Introductory Physics Problems.

Jiang, C., Shan, S., Zhou, Z., Liang, L., & Huang, H. (2019). Theoretical study of multilayer ring metamaterial emitter for a low bandgap TPV cell. *Solar Energy*, *194*, 548-553..

Jin, S., Lim, M., Lee, S. S., & Lee, B. J. (2016). Hyperbolic metamaterial-based near-field thermophotovoltaic system for hundreds of nanometer vacuum gap. *Optics express*, *24*(6), A635-A649.

Kirchhoff, G. (1978). Über das Verhältnis zwischen dem Emissionsvermögen und dem Absorptionsvermögen der Körper für Wärme und Licht. In *Von Kirchhoff bis Planck* (pp. 131-151). Vieweg+ Teubner Verlag, Wiesbaden.

Lambert, J. B., Mazzola, E. P., & Ridge, C. D. (2019). *Nuclear magnetic resonance spectroscopy: an introduction to principles, applications, and experimental methods*. John Wiley & Sons..

Landy, N. I., Sajuyigbe, S., Mock, J. J., Smith, D. R., & Padilla, W. J. (2008). Perfect metamaterial absorber. *Physical review letters*, *100*(20), 207402..

Lin, S. Y., Fleming, J. G., Chow, E., Bur, J., Choi, K. K., & Goldberg, A. (2000). Enhancement and suppression of thermal emission by a three-dimensional photonic crystal. *Physical Review B*, *62*(4), R2243..

Long, J., Xiao, M., Huang, X., Xing, Z., Li, X., Dai, P., ... & Lu, S. (2019). High efficiency thin film GaInP/GaAs/InGaAs inverted metamorphic (IMM) solar cells based on electroplating process. *Journal of Crystal Growth*, *513*, 38-42.

Maremi, F. T., Lee, N., Choi, G., Kim, T., & Cho, H. H. (2018). Design of multilayer ring emitter based on metamaterial for thermophotovoltaic applications. *Energies*, *11*(9), 2299.

Martín, D., & Algora, C. (2004). Temperature-dependent GaSb material parameters for reliable thermophotovoltaic cell modelling. *Semiconductor science and technology*, *19*(8), 1040.

Martin-Moreno, L., Garcia-Vidal, F. J., Lezec, H. J., Pellerin, K. M., Thio, T., Pendry, J. B., & Ebbesen, T. W. (2001). Theory of extraordinary optical transmission through subwavelength hole arrays. *Physical review letters*, *86*(6), 1114..

Millikan, R. A. (1916). A direct photoelectric determination of Planck's" h". *Physical Review*, *7*(3), 355.

Murdock, H. E., Gibb, D., André, T., Sawin, J. L., Brown, A., Appavou, F., ... & Mastny, L. (2020). Renewables 2020-Global status report.

Nguyen-Huu, N., Pištora, J., & Cada, M. (2016). Wavelength-selective emitters with pyramid nanogratings enhanced by multiple resonance modes. *Nanotechnology*, *27*(15), 155402.

Ni, Q., Ye, H., Shu, Y., & Lin, Q. (2016). A theoretical discussion on the internal quantum efficiencies of the epitaxial single crystal GaSb thin film cells with different p–n junctions. *Solar Energy Materials and Solar Cells*, *149*, 88-96.

Norton, B., Duffy, A., & Oubaha, M. (2017). Hybrid Solar Thermophotovoltaic-Biomass/Gas Power Generation System with a Spectrally Matched Emitter for Lower Operating Temperatures.

Oelker, G. A. S. (2019). *Thermophotovoltaic cell design improvements through numerical simulations: uncertainty quantification and geometry optimization*. Pontificia Universidad Catolica de Chile (Chile).

Omair, Z., Scranton, G., Pazos-Outón, L. M., Xiao, T. P., Steiner, M. A., Ganapati, V., ... & Yablonovitch, E. (2019). Ultraefficient thermophotovoltaic power conversion by band-edge spectral filtering. *Proceedings of the National Academy of Sciences*, *116*(31), 15356-15361.

Pfiester, N. A. (2015). *Optimization of Metamaterial Selective Emitters for Use in Thermophotovoltaic Applications* (Doctoral dissertation, Tufts University).

Rashid, W. E. S. W. A., Ker, P. J., Jamaludin, M. Z. B., Gamel, M. M. A., Lee, H. J., & Abd Rahman, N. B. (2020). Recent development of thermophotovoltaic system for waste heat harvesting application and potential implementation in thermal power plant. *IEEE Access*, *8*, 105156-105168.

Richel, A., Johnson, N. P., & McComb, D. W. (2000). Observation of Bragg reflection in photonic crystals synthesized from air spheres in a titania matrix. *Applied Physics Letters*, *76*(14), 1816-1818.

Rinnerbauer, V., Ndao, S., Yeng, Y. X., Chan, W. R., Senkevich, J. J., Joannopoulos, J. D., ... & Celanovic, I. (2012). Recent developments in high-temperature photonic crystals for energy conversion. *Energy & Environmental Science*, *5*(10), 8815-8823.

Robertson, W. M., & May, M. S. (1999). Surface electromagnetic wave excitation on one-dimensional photonic band-gap arrays. *Applied physics letters*, *74*(13), 1800-1802.

Rodriguez, A. W., Ilic, O., Bermel, P., Celanovic, I., Joannopoulos, J. D., Soljačić, M., & Johnson, S. G. (2011). Frequency-selective near-field radiative heat transfer between photonic crystal slabs: a computational approach for arbitrary geometries and materials. *Physical review letters*, *107*(11), 114302.

Ryu, H. Y., & Notomi, M. (2003). Enhancement of spontaneous emission from the resonant modes of a photonic crystal slab single-defect cavity. *Optics letters*, *28*(23), 2390-2392.

Sakakibara, R., Stelmakh, V., Chan, W. R., Ghebrebrhan, M., Joannopoulos, J. D., Soljacic, M., & Čelanović, I. (2019). Practical emitters for thermophotovoltaics: a review. *Journal of Photonics for Energy*, *9*(3), 032713..

Schock, A., & Kumar, V. (1995, January). Radioisotope thermophotovoltaic system design and its application to an illustrative space mission. In *AIP Conference Proceedings* (Vol. 321, No. 1, pp. 139-152). American Institute of Physics.

Seyf, H. R., & Henry, A. (2016). Thermophotovoltaics: a potential pathway to high efficiency concentrated solar power. *Energy & Environmental Science*, *9*(8), 2654-2665.

Shoaei, E. (2016). Performance assessment of thermophotovoltaic application in steel industry. *Solar Energy Materials and Solar Cells*, *157*, 55-64.

Smith, D. R., Schultz, S., Markoš, P., & Soukoulis, C. M. (2002). Determination of effective permittivity and permeability of metamaterials from reflection and transmission coefficients. *Physical review B*, *65*(19), 195104.

Smith, D. R., Pendry, J. B., & Wiltshire, M. C. (2004). Metamaterials and negative refractive index. *Science*, *305*(5685), 788-792.

Stelmakh, V. (2017). *A practical high temperature photonic crystal for high performance thermophotovoltaics* (Doctoral dissertation, Massachusetts Institute of Technology).

Tan, M., Ji, L., Wu, Y., Dai, P., Wang, Q., Li, K., ... & Yang, H. (2014). Investigation of InGaAs thermophotovoltaic cells under blackbody radiation. *Applied Physics Express*, *7*(9), 096601.

Teofilo, V. L., Choong, P., Chang, J., Tseng, Y. L., & Ermer, S. (2008). Thermophotovoltaic energy conversion for space. *The Journal of Physical Chemistry C*, *112*(21), 7841-7845.

Tian, Y., Ghanekar, A., Ricci, M., Hyde, M., Gregory, O., & Zheng, Y. (2018). A review of tunable wavelength selectivity of metamaterials in near-field and far-field radiative thermal transport. *Materials*, *11*(5), 862..

Tuley, R. S., Orr, J. M. S., Nicholas, R. J., Rogers, D. C., Cannard, P. J., & Dosanjh, S. (2012). Lattice-matched InGaAs on InP thermophovoltaic cells. *Semiconductor science and technology*, *28*(1), 015013.

Wanlass, M. W., Carapella, J. J., Duda, A., Emery, K., Gedvilas, L., Moriarty, T., ... & Murray, C. S. (1999, March). High-performance, 0.6-eV, Ga 0.32 In 0.68 As/InAs 0.32 P 0.68 thermophotovoltaic converters and monolithically interconnected modules. In *AIP Conference Proceedings* (Vol. 460, No. 1, pp. 132-141). American Institute of Physics.

Wolfson, R. (2011). *Energy, environment, and climate*. WW Norton & Company.

Woolf, D. N., Kadlec, E. A., Bethke, D., Grine, A. D., Nogan, J. J., Cederberg, J. G., ... & Hensley, J. M. (2018). High-efficiency thermophotovoltaic energy conversion enabled by a metamaterial selective emitter. *Optica*, *5*(2), 213-218..

Würfel, P., & Würfel, U. (2016). *Physics of solar cells: from basic principles to advanced concepts*. John Wiley & Sons.

Xuan, Y., Chen, X., & Han, Y. (2011). Design and analysis of solar thermophotovoltaic systems. *Renewable Energy*, *36*(1), 374-387.

Zhang, Z., Park, K., & Lee, B. J. (2011). Surface and magnetic polaritons on two-dimensional nanoslab-aligned multilayer structure. *Optics Express*, *19*(17), 16375-16389..

Zhao, B., Santhanam, P., Chen, K., Buddhiraju, S., & Fan, S. (2018). Near-field thermophotonic systems for low-grade waste-heat recovery. *Nano letters*, *18*(8), 5224-5230.

Zhongming, Z., Linong, L., Xiaona, Y., Wangqiang, Z., & Wei, L. (2019). Renewable Energy Now Accounts for a Third of Global Power Capacity.

Zhou, Z., Sakr, E., Sun, Y., & Bermel, P. (2016). Solar thermophotovoltaics: reshaping the solar spectrum. *Nanophotonics*, *5*(1), 1-21.